Cis-regulatory evolution of Wnt family genes contributes to a morphological difference between silkworm species

Kenta Tomihara[1,¶], Ana Pinharanda[2,3¶], Young Mi Kwon[2], Andrew M. Taverner[4], Laura S. Kors[5], Matthew L. Aardema[4,6], Julia C. Holder[2], Lin Poyraz[2], Takashi Kiuchi[1,&], and Peter Andolfatto[2,&]

[1]Department of Agricultural and Environmental Biology, Graduate School of Agricultural and Life Sciences, University of Tokyo; Yayoi 1-1-1, Bunkyo-ku, Tokyo 113-8657, Japan.

[2]Department of Biological Sciences, Columbia University; 1212 Amsterdam Avenue, New York, NY, 10027, USA.

[3]Department of Immunology and Infectious Diseases, Harvard T.H. Chan School of Public Health; Boston, MA, 02115, USA.

[4]Lewis-Sigler Institute for Integrative Genomics, Princeton University; Princeton, NJ, 08544, USA.

[5]Department of Biology, Barnard College, Columbia University; New York, NY 10027, USA

[6]Department of Biology, Montclair State University; Montclair, NJ, 07043, USA

¶ Contributed equally to this work

& Co-supervised this work.

Corresponding authors. Email: pa2543@columbia.edu, kiuchi@g.ecc.u-tokyo.ac.jp

Short title

Cis-regulatory shifts in Wnt expression drive larval appendage evolution in silkworm moths

Abstract

Closely related species often exhibit distinct morphologies that can contribute to species-specific adaptations and reproductive isolation. One example are Lepidopteran caterpillar appendages, such as the "caudal horn" of Bombycoidea moths, which have evolved substantial morphological diversity among species in this group. Using interspecific crosses, we identify the genetic basis of the caudal horn size difference between *Bombyx mori* and its closest relative *B. mandarina*. The three largest of eight QTL account for one third the mean horn length difference between the species. The largest of these, on chromosome 4, encompasses a conserved Wnt family gene cluster, key upstream regulators that are well-known for their roles in morphological diversification in animals. Using allele-specific expression analysis and CRISPR/Cas9 knockouts, we show that tissue-specific *cis*-regulatory changes to *Wnt1* and *Wnt6* contribute to the species difference in caudal horn size. This kind of modularity enables highly pleiotropic genes, including key upstream growth regulators, to contribute to the evolution of morphological traits without causing widespread deleterious effects.

Significance

This study explores the genetic basis of a distinct morphological trait that varies between two closely related moth species, providing insights into the evolution of morphological diversity. By identifying *cis*-regulatory changes in two Wnt family genes as major contributors, this work underscores the importance of developmental gene regulatory networks in shaping species-specific traits. The findings illustrate how even small modifications in major upstream regulator genes can drive significant phenotypic variation, revealing how genetic changes in key growth regulators fuel the diversification of form and function. These results advance our understanding of the mechanisms behind the evolution of complex morphological traits.

Introduction

Understanding the genetic mechanisms underlying morphological evolution has long been a central goal in evolutionary biology [1–3]. This pursuit has yielded a growing number of cases in which the genetic basis of morphological traits that differentiate populations and species has been identified [4]. However, it is increasingly clear that the genetic architecture of morphological evolution is both complex and varied. In some cases, dramatic phenotypic changes can be attributed to a few loci of large effect; in others, they involve many genes of smaller effect. Studies of the genetic basis of pigmentation trait variation between insect species, for example, often reveal a relatively simple oligogenic basis [5–7]. By contrast, the genetic foundations of more complex morphological, physiological, and behavioral traits remain less well resolved. A related debate concerns whether evolutionary changes in these complex traits are primarily driven by modifications in high-level regulatory genes or in their downstream targets, and whether regulatory or protein-coding sequence changes play the dominant role. Addressing these questions is key to building a comprehensive picture of the genetic basis of morphological evolution [8–10].

Insects have evolved a wide range of morphological adaptations, including projections used for combat [11], mate choice [12], digging [13], sensing [14], and defense [15]. Among these, lepidopteran caterpillars exhibit an impressive range of protruding structures, such as setae, spines and horns. The evolution of these structures across different species has resulted in remarkably diverse caterpillar morphologies (**Fig 1, S1**

Table). One notable example is the "caudal horn", a conspicuous fleshy projection found at the posterior end of Bombycoidea caterpillars (**Fig 1B, S1 Table**). The caudal horn exhibits substantial variation in size, shape and color among different species in the family, suggesting potential adaptive importance of this structure. Little is known about its function, but it has been speculated that in some species it may play a role in crypsis or in sensory capacity [16]. Specifically, some Bombycidae have been reported to move their caudal horn when disturbed [17]. While for other Lepidoptera, caterpillars with horn-like projections rapidly beat them when approached by parasitoids, suggesting a potential role for such horns in defense [18].

The mechanisms underlying evolutionary gains and losses of morphological innovations, like the caudal horn, are often inaccessible to genetic analysis due to reproductive barriers between species exhibiting different traits. In this study, we take advantage of the fact that the domesticated silkworm *Bombyx mori* and its closest relative *B. mandarina* (both members of the Bombycoidea group, **Fig 1**) produce fertile hybrids. *B. mori* is believed to have been domesticated ~4-10 thousand years ago [19–21] from a *B. mandarina*-like ancestor that may have started diverging from extant *B. mandarina* lineages more than 1 million generations ago [22]. During this time, *B. mori* and *B. mandarina* have diverged in a variety of morphological, physiological and behavioral traits. Several of these traits, including size, loss of flight, silk yield and larval foraging behavior are likely to be directly associated with the domestication [23–25]. However, for other traits – such as larval caudal horn length, olfactory capacity, and pigmentation – their adaptive significance remains unclear, although in the case of

pigmentation, darker coloration in *B. mandarina* may contribute to crypsis, while its reduction in *B. mori* might facilitate detection by farmers ([26–28]; **Fig 1B, S1 Table, S1 Fig**).

Given the broad diversity in larval appendages among Lepidoptera, of which diversification of the caudal horn among the Bombicoidea is a part, we use interspecific crosses and advances in high-throughput genotyping to investigate the genetic basis of the caudal horn length difference between *B. mori* and *B. mandarina*. Further, using gene expression studies and targeted knock-outs, we identify causative loci underlying the largest QTL contributing to the caudal horn length difference between species. Our work sheds light on how novel species-specific morphological traits can evolve over relatively short evolutionary timescales.

Results

Multiple QTL underlie caudal horn length divergence

The caudal horn structure on the eighth segment of *Bombyx mori* caterpillars is substantially smaller than that of its wild sister species *B. mandarina* (Fig 1B and Fig 2A inset). To quantify this difference, we measured caudal horn lengths of fifth instar larvae using a landmark-based approach (**Methods, S1A Fig**). The caudal horn of *B. mandarina* Sakado strain (3.51 ± 0.08 mm) is over 3-fold longer than that of *B. mori* p50T strain (0.94 ± 0.11 mm) (**Fig 2A**). This length difference is consistent across seven additional *B. mori* strains (**S1B Fig**). The mean caudal horn length for p50T/Sakado F1 hybrids is intermediate (2.28 ± 0.09 mm) suggesting that some alleles contributing to longer caudal horn length in *B. mandarina* are partially dominant. Within species, body size and caudal horn size exhibit positive allometry, as often observed for morphological traits. In contrast, the opposite pattern is observed between species, with *B. mori* caterpillars having a shorter horn than *B. mandarina*, despite the former being substantially larger [25] (**S1D Fig**).

To investigate the genetic basis of caudal horn length divergence between species, we generated two hybrid mapping populations. For the first, *B. mori* females were crossed with *B. mandarina* males to generate F1 hybrids, and F1 males were then backcrossed to *B. mori* females, producing a first-generation backcross (BC1) panel of 694 individuals. For the second mapping population, *B. mori* males were crossed with *B. mandarina* females to generate F1 hybrids, and F1 males and females were intercrossed to produce

an F2 panel of 327 individuals (**Methods, S2 Fig**). The phenotype distribution of BC1 progeny continuously spans the range of phenotypes between *B. mori* p50T and p50T/Sakado F1 hybrids (**Fig 2A**), as expected for trait variation that is encoded by several causative loci.

Quantitative trait locus (QTL) analyses of these two mapping populations reveal multiple loci contributing to caudal horn length divergence between species. Analysis of BC1 mapping population identifies eight QTL with significant effects on caudal horn length (**Fig 2B**). The largest effect QTL is localized to a 600 kilobase interval on chromosome 4 (Chr4). This QTL accounts for 18% of the variance among BC1 progeny and 11% of the mean length difference between species (**S2 Table**, **Fig 2C**). The three largest effect BC1 QTL (Chr4, Chr5 and Chr21) jointly account for 27% of the mean length difference between species. The remaining QTL have smaller, marginally significant effects and are less well spatially resolved (**Fig 2C**, **S2 Table**). Caterpillar weight (a proxy for size) and sex also contribute significantly to the variance in caudal horn length among BC1 progeny. Interestingly, all eight QTL have effects in the same direction, *i.e.* the *B. mandarina* allele is associated with longer mean caudal horn length (QTL Sign Test p-value =0.008; **Fig 2C**, **S3 Fig**). The biased direction of QTL effects implies that difference in caudal horn size between species is not likely to be solely attributable to genetic drift [29].

Since F1 male individuals were backcrossed only to *B. mori* females (**S2 Fig**), analysis of the BC1 panel can only detect loci for which the *B. mandarina* allele has a substantial

effect in heterozygotes. To alleviate this limitation, we performed QTL analysis of the F2 mapping population. This F2 QTL scan found only one locus with significant effects on caudal horn length, Chr4 (**S3 Table**, **S3 Fig**), which overlaps the largest QTL observed in the BC1 analysis and shows consistent effect size with the BC1 Chr4 QTL. The effect size of the F2 Chr4 QTL is consistent with the findings from the BC1 cross. Furthermore, we independently verified the Chr4 QTL by phenotyping consomic (and semi-consomic) introgression strains of Chr4 (see **S4 Fig**). Conspicuously absent from the F2 QTL scan are the additional QTL detected in the BC1 mapping panel. The smaller mapping panel for the F2 analysis may explain the relatively coarse spatial resolution of the Chr4 QTL and the absence of the seven other QTL detected in the BC1 analysis. However, the proportion of *B. mandarina* ancestry on BC1 QTL-bearing chromosomes — excluding Chr4— is a significant predictor of caudal horn length (**S3 Table**, p-value = 3.4e-7), suggesting that loci on these chromosomes contribute to the trait difference despite not reaching significance in the F2 QTL analysis.

Evidence for additional loci beyond mapped QTL

The above analyses provide strong evidence for at least eight loci contributing to the caudal horn length difference between species. However, how many more loci might contribute remains unclear. Notably, the proportion of *B. mandarina* ancestry on the remaining non-QTL-bearing chromosomes is also a significant predictor of caudal horn length in the F2 mapping panel (**S3 Table**, p-value = 4.3e-10), consistent with a model in which many small effect loci also contribute to the morphological difference between species. To investigate this further, we carried out a regression analysis of caudal horn

length as a function of per chromosome *B. mandarina* ancestry (**S5 Fig**). This analysis reveals that the proportions of *B. mandarina* ancestry on Chr3 and Chr6 are significant predictors of increased caudal horn length in the BC1 mapping panel, in addition to the QTL already identified by QTL mapping (**S5 FigB**). Even after accounting for QTL-bearing chromosomes, a significant positive correlation between caudal horn length and *B. mandarina* ancestry persists in the F2 mapping population. This indicates that additional small-effect caudal horn-shortening alleles on non-QTL-bearing chromosomes have accumulated in the *B. mori* lineage. We estimate that *B. mandarina* ancestry on non-QTL bearing chromosomes accounts for 8.5% of the variance among F2 caudal horn lengths (**S3 Table**). Thus, while the horn trait difference is clearly dominated by an oligogenic architecture, an unknown number of additional loci on non-QTL bearing chromosomes also make a substantial contribution to variation in this trait.

Two Wnt family genes exhibit caudal horn-specific *cis*-regulatory evolution

The 1.5 LOD (Logarithm of the Odds) interval for the BC1 Chr4 QTL region contains 17 annotated genes (**S4 Table**). Among these is a cluster of four Wnt family genes (**Fig 2D**), a family of secreted growth factor proteins with diverse roles in morphological development in animals [30,31]. *Wnt* genes are highly conserved across animals, and this cluster (*Wnt9*, *Wnt1*, *Wnt6* and *Wnt10*) is syntenic with orthologous genes in the *Drosophila melanogaster* genome (**S4 Table**). The QTL region is syntenic in the two *Bombyx* species, with no evidence of an inversion or large insertions/deletions.

Given the presence of the *Wnt* gene cluster in the Chr4 QTL region, we speculated that differences in tissue-specific regulation of one or more of these *Wnt* genes may account for species differences in caudal horn size. To test this hypothesis, we investigated patterns of tissue-specific expression for 17 genes in the Chr4 QTL 1.5 LOD interval. First, we carried out RNA-seq to identify segment-specific differential expression between the two species (**S5 Table**). We examined early-stage caterpillars (second instar, L2) because the difference in caudal horn length between the species is already visible when they hatch (**S1C Fig**), becoming more pronounced in later larval stages (**S1A and S1D Figs**). We detected 1306 transcripts with segment-specific expression divergence between species (**Supplemental Data 2**). Out of these, 121 transcripts overlap the identified QTL regions. Interestingly, this analysis reveals that only *Wnt6* exhibits significant species- and tissue-specific differential expression, with a two-fold upregulation in the eighth abdominal (A8) segment of *B. mandarina* relative to *B. mori* in the Chr4 QTL (**S6 FigA, S5 Table**).

However, bulk-tissue RNA-seq-based differential expression analysis has limited statistical power for genes with low expression levels like this Chr4 cluster of Wnt family genes (**S6 FigA**). Moreover, between-species comparisons of gene expression can be difficult to interpret due to species-specific differences in the *trans*-regulatory environment and other differences in development (e.g. cell number, the timing of development, etc.). To identify genes with *cis*-regulatory divergence between species,

we examined allele-specific expression (ASE) in F1 hybrids, which compares the expression of two alleles in a common *trans*-environment [32].

To assay ASE, we used a targeted PCR-based approach (see Methods). We further dissected the A8 segment into the caudal horn structure itself (CH) versus the remaining "non-horn" A8 tissue, with the goal of improving tissue resolution beyond the level of segment (**Fig 3A**). This analysis reveals that only two genes, *Wnt1* and *Wnt6*, exhibit caudal horn-specific allele-specific expression in the fifth instar (L5) of F1 hybrid caterpillars (**Fig 3B**, **S6 Table**). Specifically, both genes exhibit a caudal horn-specific down-regulation of the *B. mori* allele relative to the *B. mandarina* allele. A similar trend is observed in the F1 hybrid caterpillars at the first instar (L1) stage when the between-species caudal horn length difference is less pronounced (**S6 FigB; S6 Table**). gDNA samples from F1 hybrids were processed in the same way as cDNA, and in all cases the *B. mandarina*:*B.mori* allele ratios did not differ significantly from 1, confirming the absence of amplification bias (see methods for details, **Supplemental Data S3**). These results show that the *cis*-regulatory elements of *Wnt1* and *Wnt6* have diverged between these species, suggesting that differences in their tissue-specific expression may contribute to the species difference in caudal horn length. Notably, the Wnt1 and Wnt6 proteins of *B. mori* and *B. mandarina* are identical in amino acid sequence, indicating that any functional differences between the species involving these genes are solely due to *cis*-regulatory differences in gene expression (**S4 Table**).

To examine temporal patterns of *Wnt1* and *Wnt6* expression, we used reverse transcription quantitative PCR (RT-qPCR) to measure relative transcript abundance in integumentary tissue from caudal-horn bearing and control segments (A8 and A7, respectively) of *B. mori* and *B. mandarina*. This analysis (**Fig 3C**; **S6C Fig**) revealed several species- and tissue-level differences in expression dynamics. First, both *Wnt1* and *Wnt6* are generally expressed at higher levels in the caudal horn bearing A8 segment. Second, expression of both genes is consistently higher in *B. mandarina* than in *B. mori*, especially in the A8 segment. Third, this species difference emerges earlier for *Wnt6* and peaks for both genes at the onset of the molt preceding the L5. These findings suggest that allele-specific expression differences measured during the fifth instar (**Fig 3B**) may underestimate the divergence present at the end of the fourth instar. Specifically, *Wnt1* expression was highest in the caudal segments of *B. mandarina* on day 3 of the fourth instar, and at this time point *Wnt1* levels were also elevated in the caudal segments of both species relative to non-caudal segments. Together, the results support the idea that reduced *Wnt1* and/or *Wnt6* expression in the caudal segment of *B. mori* may contribute to its shorter horn phenotype.

At the L5 stage, species-level expression differences (**Fig 3C**) closely match allele-specific expression differences measured in the caudal horn of F1 hybrids (**Fig 3B**). Notably, the differential expression *Wnt1* exhibits 2.3-fold higher expression in *B. mandarina* relative *to B. mori*, compared to a 2.2-fold *B. mandarina*-allele bias in F1 hybrids. Similarly, *Wnt6* exhibits 3.1-fold higher expression in *B. mandarina* relative *to B. mori* and a 3.0-fold *B. mandarina*-allele bias in F1 hybrids. This concordance indicates

that *cis*-regulatory divergence is sufficient to explain most of the observed species-level expression differences for both genes, with little evidence for an important *trans*-regulatory contribution.

Functional analyses reveal that *Wnt1* and *Wnt6* contribute to caudal horn length evolution

While we have established that both *Wnt1* and *Wnt6* are down-regulated in the caudal horn of *B. mori* relative to *B. mandarina*, expression studies alone cannot determine whether one or both genes have a causal effect on horn growth. Thus, to functionally validate the role of *Wnt1* and *Wnt6* in the evolved caudal horn difference between species, we used allele-specific CRISPR/Cas9-mediated gene knockouts of *B. mandarina* alleles [26]. We crossed injected (G0) females of semi-consomic line T04 ($chr4^{mand}/chr4^{mori}$) to *B. mori* p50T males to generate G1 larvae. G1 females whose *B. mandarina*-derived *Wnt1* or *Wnt6* is disrupted by small frameshift causing premature stop codon were crossed to p50T males to establish *B. mandarina*-allele-specific knockout mutants (**S7 Fig**). Knocking out the *B. mandarina*-derived allele of *Wnt1* in hybrids results in a 51% reduction in caudal horn length (Tukey's HSD, $p<0.001$; **Fig 4A**). Knocking out the *B. mandarina*-derived allele of *Wnt6* also results in a reduction in horn length, but the effect (a 7% reduction) is substantially smaller (Tukey's HSD, $p<0.05$; **Fig 4A**). Notably, with the exception of caudal horn length, we did not notice any pigmentation or morphological changes in larvae with *Wnt1* and *Wnt6* knock-outs. If *B. mori* represents the derived state, our results suggest that the down-regulation of

295 *Wnt1* in *B. mori* contributes substantially to its reduced caudal horn length relative to *B. mandarina* (**Fig 4B**).

Discussion

The role of Wnt1 and Wnt6 in morphological divergence between species

We investigated the molecular mechanisms underlying the diversification of a conspicuous larval appendage structure, the caudal horn, in Bombycoidea caterpillars. Our findings highlight how morphological divergence between species can result from tissue-specific regulatory changes affecting major upstream developmental genes. Specifically, we show that *cis*-regulatory downregulation of two Wnt family genes, *Wnt1* and *Wnt6*, in the developing caudal horn of *B. mori* is the single largest contributing factor to the reduction in caudal horn length in this species. Although our analyses focus on later larval stages, reduced horn length in *B. mori* relative to *B. mandarina* is already evident at the neonate stage (**S1 Fig**), suggesting that the causal regulatory differences arise earlier in development, potentially during embryogenesis.

Wnt family genes are well known for their roles in limb and appendage development [30,33,34] and, more broadly, Wnt signaling is associated with cell proliferation and tissue growth across many developmental contexts [35,36]. Despite this, there are few clear examples in which evolutionary changes to Wnt genes themselves drive morphological evolution. Prior work has shown that *cis*-regulatory evolution of *Wnt1* and *WntA* can underlie pigmentation differences among insect species [37–39] . Beyond pigmentation differences, recent work in *Heliconius* butterflies [40] and *B. mori* [41] showed that Wnt signaling can modulate appendage extension through regulation of the downstream transcription factor *aristaless*. However, whether these effects are

mediated by *cis*-regulatory changes at Wnt family genes remains unclear. To our knowledge, the role of *Wnt1* and *Wnt6* in *Bombyx* caudal horn divergence is the first example in which *cis*-regulatory evolution at Wnt family genes has been directly linked to divergence in a morphological structure (**S7 Table**).

The regulation of expression and functional roles of Wnt family genes are diverse and complex across animals [42–44]. In insects, *Wnt1* and *Wnt6* share high sequence similarity, are physically adjacent in the genome, and exhibit overlapping expression domains. These features have led to the hypothesis that the two genes are at least partially co-regulated and may act redundantly in some developmental contexts [39,45,46]. Consistent with this view, a shared enhancer for *Wnt1* and *Wnt6* has been identified in *D. melanogaster* [47]. Since both *Wnt1* and *Wnt6* are downregulated in the *B. mori* caudal horn relative to *B. mandarina*, it may be that the causal cis-regulatory changes involve a shared horn-specific enhancer. Allele-specific knockouts further reveal that both *Wnt1* and *Wnt6* contribute to horn development—though to differing degrees—supporting the idea of partial redundancy (**Fig 4**). The larger effect of *Wnt1* on caudal horn size in allele-specific knockout experiments suggests that it is more functionally potent or dosage-sensitive in this context.

Together, these findings add to a small but growing list of examples showing that *cis*-regulatory changes in major upstream developmental genes can underlie morphological differences, beyond pigmentation traits, between closely related species and domesticated animals (**S7 Table**). Our results also underscore how regulatory modularity enables the resolution of developmental trade-offs associated with

morphological trait divergence. The tissue-specific downregulation observed in *B. mori* illustrates how spatially restricted regulatory changes can decouple traits, allowing selection to act on horn size without potentially negative pleiotropic effects. Such modularity is a key feature of evolvability and exemplifies the utility of tissue-specific enhancers in facilitating adaptive change.

Large effect loci contribute to the evolution of the caudal horn in *Bombyx*

Although domestication differs from natural selection, it nonetheless offers a powerful framework for studying rapid evolutionary change under strong and often directional selective pressures [48]. While some domestication traits are Mendelian, others involve more complex, quantitative architectures. Our QTL mapping analysis suggests that, in addition to *Wnt1/Wnt6*, at least seven more loci with smaller effects contribute to horn length variation. The three largest QTL jointly account for 27% of the difference in mean caudal horn between species, indicating that multiple loci of moderate-to-large effect explain a substantial portion of the phenotype. The oligogenic architecture of this domestication-associated trait difference resembles that of at least some traits shaped by natural selection, such as pelvic spine reduction in stickleback [49] and sexually dimorphic pigmentation in *Drosophila* [50].

Additionally, we find that QTL loci act in concert with a substantial measurable genetic component residing outside of mapped QTL loci. This finding raises the question of the true degree of polygenicity of the caudal horn trait difference. Seven of the eight

detected QTL have small estimated effect sizes, likely reflecting loci with true effect sizes that are even smaller [51,52] and close to the threshold of detectability for this mapping panel. This implies that true number of contributing loci could be substantially larger. While few studies have quantified the relative contribution of the genomic background in detail, it is increasingly likely that a substantial contribution small effect loci to trait differences is a common, if often overlooked, feature of morphological divergence between species (see, for example, [53]).

Evolutionary forces shaping caudal horn evolution

The selective pressures driving caudal horn reduction in *B. mori* remain uncertain. Direct selection on horn length during domestication is unlikely. However, the consistent direction of effect across all eight QTL—where *B. mandarina* alleles increase horn length—argues against a purely neutral model [29,54]. One possibility is that horn reduction occurred as a correlated response to selection on other traits. Alternatively, the horn may have become maladaptive in the domesticated environment. The repeated gain and loss of horn-like structures across wild Bombycoidea species suggests that natural selection has repeatedly acted on this trait, potentially targeting similar developmental pathways.

Changes in Wnt family gene expression have previously been implicated in morphological differences among closely-related species [37–39,55]. In Lepidoptera, *Wnt1* expression has been linked to variation in pigmentation [56] and to the formation of protruding structures [57]. Our results extend these findings by

showing that tissue-specific downregulation of *Wnt1* in the developing caudal horn, also a protruding structure in caterpillars, is linked to cis-regulatory evolution of *Wnt1* itself, rather than changes to *trans*-acting factors [57] . Our results extend these findings by showing that tissue-specific downregulation of Wnt1 in the developing caudal horn, also a protruding structure in caterpillars, is linked to cis-regulatory evolution of Wnt1 itself, rather than changes to trans-acting factors. A key next step will be to identify the precise cis-regulatory elements responsible for *Wnt1* / *Wnt6* downregulation in *B. mori*. It is plausible that similar regulatory modules have been repeatedly co-opted for morphological innovation across Lepidoptera (**Fig 1**). Comparative studies in other species could reveal whether parallel evolution of Lepidopteran morphology has been driven by convergent changes in *Wnt* gene regulation.

Conclusion

This study integrates quantitative genetics with functional analyses to reveal the molecular basis of a conspicuous morphological trait difference distinguishing closely related species. We demonstrate that spatially precise regulatory changes in key developmental genes—*Wnt1* and *Wnt6*—underlie horn reduction in *B. mori*. These results highlight how cis-regulatory evolution can drive morphological divergence while minimizing pleiotropic effects, emphasizing the role of enhancer modularity in enabling adaptive evolution. This principle is likely to be broadly applicable across systems and taxa in evolutionary developmental biology.

Materials and Methods

Phylogenetic relationships

A cladogram for representative Lepidopteran species was constructed based on phylogenetic reconstructions of the Noctuoidea [58] the Bombicoidea [59] and the Papilonidea [60] and a broader phylogeny including all three groups [61] . A cladogram for the Bombicidae was reconstructed based on several recent phylogenetic reconstructions of members of this group [62–64].

Sample collection

Bombyx mori strains c51, f35, g53, o56, p20, p21, p22, T04, and CT04 were provided from Kyushu University supported by the National BioResource (https://shigen.nig.ac.jp/silkwormbase/). *B. mori* strain p50T and *B. mandarina* strain Sakado were maintained at the University of Tokyo. For the BC1 mapping panel, F1 males were generated by crossing *B. mori* (p50T) females to *B. mandarina* (Sakado) males (**S2 Fig**). We crossed F1 males to females *B. mori* p50T, generating BC_1 progeny. For the F2 mapping panel, *B. mori* p50T males were crossed with to *B. mandarina* Sakado females to produce an F1 generation, and then F1 males and females were crossed to produce an F2 generation (**S2 Fig**). We phenotyped and genotyped 696 BC1 and 327 F2 caterpillars as outlined below.

Rearing and phenotyping

Larvae were reared on white mulberry (*Morus alba*) leaves or an artificial diet SilkMate PS (Nosan, Japan) at 25 ºC with a 12-hour light: 12-hour dark light cycle. We weighed and photographed fifth instar larvae at day 0 for subsequent phenotyping. Caudal horn lengths were measured from photographs by marking two points at the base of the horn and a third point at the tip of the horn using either a custom MATLAB script or ImageJ [65]. The microscope S9D (Leica Microsystems, Germany) equipped with a MC 170 HD camera (Leica Microsystems) was used to take photographs. For each horn, we defined a triangle extending upward from the base of the horn using three points (1, 2, 3), and an additional segment defined by a 4th point at the center of the horn (**S1A Fig**). Length (L) was then calculated as,

$$L = \frac{|(X_2 - X_1)(Y_1 - Y_3) - (X_1 - X_3)(Y_2 - Y_1)|}{\sqrt{(X_2 - X_1)^2 + (Y_2 - Y_1)^2}} + \sqrt{(X_4 - X_3)^2 + (Y_4 - Y_3)^2},$$

where X_k and Y_k are coordinates of point k. The phenotype distributions of the BC1 and F2 are consistent with normal distributions (Shapiro-Wilk test p = 0.14 and p = 0.10, respectively).

Genome-wide ancestry assignment

We used Multiplexed Shotgun Genotyping [66] to carry out genome-wide ancestry assignment of recombinant progeny. Genomic DNA was extracted from the legs of the adults using the Quick-DNA extraction kit (Zymo Research, USA). Whole genome short-read Illumina-style libraries were generated using a Tn5-based “tagmentation” method [67]. For each individual, 4–15 ng of genomic DNA (measured using Synergy MX Microplate Reader [BioTek, USA]) was digested with Tn5 that was pre-charged

with Illumina-style adapters. Individuals were indexed by PCR amplification (18 cycles) using combinations of Illumina-compatible i5 and i7 indexed PCR primers. Library sequencing for BC1 was performed on HiSeq 2500 (Illumina, USA) at the Princeton University Genomics Core Facility, yielding 75 nucleotide single-end reads. Libraries for the F2 were sequenced on a HiSeq 4000 (Illumina, USA) at the Weill-Cornell Medical College Genomics Resources Core Facility, yielding 150 nucleotide paired-end reads, and read 1 was used for downstream analysis. Reads were de-multiplexed and adapters removed using Trim Galore (bioinformatics.babraham.ac.uk/projects/trim_galore/). The average number of reads per individual was 572,000 and individuals with fewer than 100,000 reads were discarded.

A *B. mori* p50T strain genome assembly (BHWX01000001-BHWX01000696, 2016) from Silkbase [68], and a *B. mandarina* Sakado strain genome assembly (GCA_030267445.2, NCBI) were used as parental reference genomes. Repetitive regions were identified and masked in the *B. mori* and *B. mandarina* genomes using RepeatMasker v4.1.2 with the species set to “bombyx”. We also masked sites that were polymorphic in either p50T or Sakado strains. To identify polymorphic sites within each strain, paired-end short-read Illumina reads of a p50T male (DRR064025; NCBI) and two Sakado samples (DRR059710, DRR093001; NCBI) were adapter-trimmed using Trim Galore v0.6.10 and aligned to the *B. mori* genome (bwa v0.7.17) [69] and variants were called using bcftools mpileup v1.16 [70] . Sites were removed based on the following quality filters: MQ <30, GQ<25, removing any SNPs within 5 bp of an indel (--SnpGap 5:indel), and

where the read-depth was less than half (<0.5x) or more than two times (>2x) the average total read depth.

MSG was run with *B. mori* designated as parent1 and *B. mandarina* as parent2, using the following parameters: deltapar1 = 0.01, deltapar2 = 0.05, recRate = 28, rfac = 0.0001, and priors set to (0.25, 0.5, 0.25) for F2 crosses and (0, 0.5, 0.5) for BC1 crosses. For each individual, genotypes were assigned as missing (i.e., "NA") if the posterior probability was below 90%. Additionally, we masked genomic regions between ancestry switches within an individual that occurred less than 1 Mbp apart. Finally, sites with more than 20% missing genotypes across individuals within each cross. This filtering yielded a set of 1,595,348 markers shared between the BC1 and F2 datasets. To reduce redundancy, we applied marker thinning using pull_thin (https://github.com/andrewtaverner/pull_thin) with the following settings: numMarkers = 5000, ignoreNan = True, exclude_ambiguous_AIMs = True, and autosome_prior = NA. A final set of 140,000 markers was retained for QTL analysis.

Quantitative Trait Locus (QTL) analysis

We performed two separate QTL analyses using R/qtl [71] with genotype and caudal horn lengths for 327 F2 and 694 BC1 individuals. The Haley-Knott regression method [72] was used for QTL mapping with sex, weight (a proxy for size), and genome-wide *B. mandarina* ancestry as covariates. Ancestry was calculated as the proportion of the genome assigned as *B. mandarina*-derived accounting for diploidy and regions with missing genotypes. Ancestry was calculated excluding chromosomes that carried a

significant QTL. Genome-wide 5% significance thresholds were determined by 1000 phenotype permutations [73]. These were estimated as LOD > 3.03 and LOD > 3.63 for the BC1 and F2 analyses, respectively. For each significant QTL, a 1.5 LOD support interval spanning the maxLOD peak was considered the candidate region [74]. Variance explained was calculated using the function fitqtl [71].

Differential Expression analysis

Caudal and non-caudal segments (A8 and A7, respectively; **Fig 3B**) were dissected from caterpillars before the onset of the second (L2) instar. Three replicate pools of eight individuals were generated for each species and segment (except the *B. mori* non-caudal segments, for which there are two replicates). Samples were stored at –80ºC in RNAlater (Thermo Fisher Scientific). RNA was extracted using the RNAeasy kit (QIAGEN) and RNA-seq libraries were prepared using TruSeq RNA Library Preparation Kit v2 (Illumina). Libraries were sequenced on HiSeq 4000 (Illumina) at the Weill-Cornell Medical College Genomics Resources Core Facility, yielding 312 million 150 nucleotide single-end reads. This corresponds to an average of 28 million reads per replicate and tissue. Reads were mapped to the *B. mori* annotated transcriptome [68] using STAR [75] . Read count output from STAR was then imported into DESeq2 [76] for differential expression analysis.

Differential expression analysis was performed to detect transcripts with caudal (A8) and non-caudal (A7) segment-specific expression differences between the species. To this end, the model used to analyze all tissue samples from all replicates was:

~Species:Replicate + Species*Tissue, where "Species" is *B. mori* or *B. mandarina* and "Tissue" is caudal (A8) or noncaudal (A7). The first term of the model defines Replicate as a nested variable within Species and accounts for the fact that caudal and non-caudal segments were sampled from the same individuals. Our quantity of interest is the second term, which accounts for potential interactions between Species and Tissue (i.e. species- and tissue-specific differential expression).

Allele-specific expression (ASE) analysis

To investigate allele-specific expression patterns for the genes within the Chr4 QTL, we extracted RNA from relevant tissues in B. mori p50T × B. mandarina Sakado F1 hybrids. The caudal segment (A8) was dissected from first (L1) and fifth (L5) larval instars and further dissected into caudal horn (CH) and "non-horn" A8 tissue (**Fig 3B**). Four replicate pools of 10 individuals were sampled for each segment and instar. Samples were stored in RNAlater Stabilization Solution (Thermo Fisher Scientific), and total RNA was extracted using TRIzol (Thermo Fisher Scientific), RNeasy columns (QIAGEN) and DNaseI (Thermo Fisher Scientific). Total RNA from each sample was used to create cDNA using SuperScript IV VILO (Thermo Fisher Scientific). The conversion to cDNA was repeated three times for each sample, representing technical replicates.

We quantified relative allele abundance using a targeted multiplexed PCR-sequencing approach. For each of 13 genes in the Chr4 QTL interval we tested (see **S4 Table**), PCR primers were designed to target a genic region that spans at least one SNP

distinguishing the two species (S8 Table). We PCR-amplified these amplicons from F1 cDNA samples using the following reaction conditions: 94 °C (30”), 95 °C (15”), 60 °C (30”), 68 °C (45”), 68 °C (5’) for 15 cycles. To allow multiplexed Illumina sequencing, we incorporated a second set of universal i5 and i7 Illumina-style indexes using the following conditions: 72 °C (3’), 94 °C (10”), 62 °C (15”), 68 °C (30”), 68 °C (5’) for 12 cycles. After removing primer dimers with DNA clean & concentrator (D4030), indexed amplicons were pooled and sequenced on a MiSeq (Illumina) using Reagent Micro Kit v2 (Illumina), 300 Cycles (MS-103-1002). Reads were demultiplexed and, for each replicate, we counted the number of reads corresponding to each species-specific SNP.

Genomic DNA (gDNA) was extracted from the same F1 hybrid design as the RNA samples, consisting of four replicate pools of 10 individuals each, using the DNeasy Blood & Tissue Kit (QIAGEN) and assayed using the same primer pairs to test for amplification bias. Allele counts from gDNA did not deviate significantly from a 1:1 *B. mandarina* to *B. mori* ratio (two-sided binomial tests, $P > 0.05$ in all cases), confirming the absence of systematic bias. For cDNA, allele-specific expression was quantified as log•(*B. mandarina*/*B. mori*) per replicate and means ±2SE were reported for visualization. To formally test whether allele ratios differed between caudal-horn and non-horn tissues, we used the inverted beta-binomial (IBB) test for paired-count data [73] as implemented in the R countdata package, comparing four caudal cDNA replicates against four non-caudal replicates per gene. P-values were corrected using Benjamini–Hochberg procedures. This analysis was used both to confirm whether cDNA allele ratios deviated from the gDNA-derived expectation of 1:1 and to identify significant

differences between caudal horn and non-horn tissues. The data relevant to this analysis can be found in DOI 10.5281/zenodo.17833042.

To assess whether genes within the QTL interval differed at the amino-acid level between *B. mori* and *B. mandarina*, we compared protein sequences derived from multiple genome assemblies (*B. mori*: GCF_014905235.1; *B.mandarina*: GCF_003987935.1, GCA_030267445.2). In addition, *B. mandarina* protein predictions were generated by lifting *B. mori* gene annotations onto the *B. mandarina* reference genome (GCA_030267445.2) using liftOver [77] and, where necessary, by reciprocal Exonerate [78] alignments to confirm orthology and exon structure. Protein sequences were aligned using MUSCLE [79], and alignments were inspected in SeaView [80] to identify candidate amino-acid substitutions between species. For each gene, substitutions were evaluated across assemblies. Putative amino-acid differences that were not consistently supported across *B. mandarina* genome assemblies, that had exon annotation differences, or that were absent from short-read sequencing data were considered likely annotation artefacts and excluded from further analysis. Only amino-acid substitutions supported by multiple assemblies were retained.

Reverse Transcription quantitative PCR (RT-qPCR)

To quantify the relative abundance of *Wnt1* and *Wnt6* RNA in a time course of larval development, we used a RT-qPCR approach. Total RNA was isolated from integuments

of caudal (A8) and non-caudal (A7) segments of *B. mori* and *B. mandarina* using TRIzol (Thermo Fisher Scientific). Reverse transcription was performed using the oligo (dT) primer and avian myeloblastosis virus Reverse Transcriptase contained in the RNA PCR kit (TaKaRa, Japan). We conducted RT-qPCR using the Kapa SYBR FAST qPCR kit (Kapa Biosystems, USA) and StepOnePlus Real-time PCR System (Applied Biosystems, USA). RNA abundance is quantified relative to *ribosomal protein 49* (*rp49*). Primer sets are listed in **S9 Table**.

CRISPR/Cas9-mediated allele-specific knockouts

To evaluate the effects of *Wnt1* and *Wnt6* expression on caudal horn development, we used CRISPR/Cas9-mediated allele-specific knockout approach [26]. Instead of F1 hybrids, we instead used the T04 semi-consomic strain, which is heterozygous *B. mori* (p50T) / *B. mandarina* (Sakado) for Chr4 in an otherwise *B. mori* (p50T) genomic background ([81] ; see **S4 Fig**).

We identified Cas9 PAM-sites that differed in sequence between *B. mori* and *B. mandarina* and designed CRISPR-RNA (crRNA) targeting *B. mandarina*-specific sequences (**S6 Fig**) [26]. To obtain non-diapausing eggs, we first incubated T04 eggs at 15ºC under continuous darkness until they hatch [82]. The hatched larvae were then reared under continuous 16h-light/8h-dark at 25 °C and crossed adult females to p50T males and collected fertilized eggs. A mixture of crRNA (200 ng/•L; FASMAC, Japan), *trans*-activating crRNA (tracrRNA) (200 ng/•L; FASMAC), and Cas9 Nuclease protein NLS (600 ng/•L; NIPPON GENE) was injected into eggs within 3 hours of oviposition

[83]. Injected embryos were then incubated at 25 °C in a humidified Petri dish until hatching. Adult generation 0 (G0) females were crossed with the wild-type p50T males to obtain generation 1 (G1) progeny. Genomic DNA was extracted from the G1 individuals by the HotSHOT method [84], and PCR was performed using KOD One (TOYOBO, Japan) or MightyAmp DNA Polymerase Ver.3 (TaKaRa). Mutations at the targeted site were detected by heteroduplex mobility assay using the MultiNA microchip electrophoresis system (SHIMADZU, Japan) with the DNA-500 reagent kit [85,86]. The PCR products were also cloned into pGEM-T Easy Vector (Promega, USA) and Sanger-sequenced using the FASMAC sequencing service. G1 females carrying a 7-nucleotide deletion in *B. mandarina*-derived *Wnt1* and 2-nucleotide deletion in *B. mandarina*-derived *Wnt6* were crossed to wild-type p50T males, respectively, to establish *B. mandarina*-allele-specific knockout mutants (**S7 Fig**). Both mutations result in frameshifts and premature stop codons. Mutant larvae were weighed and the caudal horn length measured as described above and then genotyped using PCR. RNA oligos and PCR primer sets were listed in **S10 Table**.

Effects of chromosome-level ancestry on caudal horn length

We analyzed ancestry and its relationship to caudal horn length using the standardized coefficients from the linear regression model as measures of effect size (R v.4.0.2). Bayesian information criterion (BIC) model selection was used to evaluate the association between ancestry and caudal horn length (**S5 Fig**) with ancestry on all chromosomes included as independent variables. We adjusted p-values using a Bonferroni correction for the 27 chromosomes tested.

Acknowledgments

M. Gutin laid the preliminary groundwork for the project as part of her Ph. D. dissertation **[87]**. We thank L. Ruiz and N. Sparman for help with insect husbandry and M. Rebeiz, T. Shimada and S. Shigenobu for helpful comments during the course of the project. We also thank the Institute for Sustainable Agro ecosystem Services, the University of Tokyo, for facilitating the mulberry cultivation and the Biotron Facility at the University of Tokyo for rearing the silkworms.

Funding

This work was supported by National Institutes of Health grants R01 GM112758, R01 GM114093, and R01 GM115523 from the National Institute of General Medical Sciences to PA, and by JSPS KAKENHI grant numbers JP20J22954 to KT and JP20H02997 to TK. The funders had no role in study design, data collection and analysis, decision to publish, or preparation of the manuscript. PA and AMT received salary support from NIH grants R01 GM112758, R01 GM114093, and R01 GM115523. AP received salary support from NIH grants R01 GM112758 and R01 GM115523. YMK received salary support from NIH grant R01 GM115523. KT received salary support from JSPS KAKENHI grant JP20J22954, and TK received salary support from JSPS KAKENHI grant JP20H02997.

Author contributions

Designed research (KT,AP,TK,PA); Performed research (KT, AP, YK, MLA, JCH, LSK, LP, AMT); Analyzed data (KT ,AP ,YK ,AMT, PA); Wrote the paper (KT, AP, TK, PA).

Competing interests

The authors declare no competing interests.

Data and materials availability

Code and analysis scripts as well as Supplemental Data tables are available at DOI 10.5281/zenodo.17833042. Whole-genome sequencing data available in the NCBI Sequence Read Archive under BioProject accession PRJNA1380446. Allelic-specific expression amplicons and corresponding metadata can be found in DOI 10.5281/zenodo.17833042.

Supplementary Materials

S1 to S7 Figs

S1 to S10 Tables

S1 to S5 Data

References

1. Shubin N, Tabin C, Carroll S. Fossils, genes and the evolution of animal limbs. Nature. 1997;388: 639–648. doi:10.1038/41710

2. Carroll SB, Grenier JK, Weatherbee SD. From DNA to diversity□: molecular genetics and the evolution of animal design. 2nd ed. Blackwell, editor. Oxford: Blackwell; 2004.

3. Davidson EH, Peter IS. Genomic Control Process: Development and Evolution. Academic Press; 2015.

4. Courtier-Orgogozo V, Arnoult L, Prigent SR, Wiltgen S, Martin A. Gephebase, a database of genotype–phenotype relationships for natural and domesticated variation in Eukaryotes. Nucleic Acids Res. 2020;48: D696–D703. doi:10.1093/nar/gkz796

5. Wittkopp PJ, Beldade P. Development and evolution of insect pigmentation: Genetic mechanisms and the potential consequences of pleiotropy. Semin Cell Dev Biol. 2009;20: 65–71. doi:10.1016/j.semcdb.2008.10.002

6. Massey JH, Wittkopp PJ. Chapter Two The Genetic Basis of Pigmentation Differences Within and Between Drosophila Species. Curr Top Dev Biol. 2016;119: 27–61. doi:10.1016/bs.ctdb.2016.03.004

7. McMillan WO, Livraghi L, Concha C, Hanly JJ. From Patterning Genes to Process: Unraveling the Gene Regulatory Networks That Pattern Heliconius Wings. Front Ecol Evol. 2020;8: 221. doi:10.3389/fevo.2020.00221

8. Orr HA, Coyne JA. The genetics of adaptation: a reassessment. Am Nat. 1992;140: 725–42. doi:10.1086/285437

9. Stern D. Evolution, development, and the predictable genome. Roberts and Company Publishers; 2010.

10. Martin A, Orgogozo V. THE LOCI OF REPEATED EVOLUTION: A CATALOG OF GENETIC HOTSPOTS OF PHENOTYPIC VARIATION. Evolution. 2013;67: 1235–1250. doi:10.1111/evo.12081

11. Emlen DJ, Marangelo J, Ball B, Cunningham CW. DIVERSITY IN THE WEAPONS OF SEXUAL SELECTION: HORN EVOLUTION IN THE BEETLE GENUS ONTHOPHAGUS (COLEOPTERA: SCARABAEIDAE). Evolution. 2005;59: 1060–1084. doi:10.1111/j.0014-3820.2005.tb01044.x

12. David P, Bjorksten T, Fowler K, Pomiankowski A. Condition-dependent signalling of genetic variation in stalk-eyed flies. Nature. 2000;406: 186–188. doi:10.1038/35018079

13. HASHIMOTO K, HAYASHI F. Structure and function of the large pronotal horn of the sand□living anthicid beetle Mecynotarsus tenuipes. Èntomol Sci. 2012;15: 274–279. doi:10.1111/j.1479-8298.2012.00517.x

14. Kandori I, Tsuchihara K, Suzuki TA, Yokoi T, Papaj DR. Long Frontal Projections Help Battus philenor (Lepidoptera: Papilionidae) Larvae Find Host Plants. PLoS ONE. 2015;10: e0131596. doi:10.1371/journal.pone.0131596

15. Kandori I, Hiramatsu M, Soda M, Nakashima S, Funami S, Yokoi T, et al. Long horns protect Hestina japonica butterfly larvae from their natural enemies. Sci Rep. 2022;12: 2835. doi:10.1038/s41598-022-06770-y

16. Packard, Cockerell. Monograph of the Bombycine Moths of North America: Family Ceratocampidæ, subfamily Ceratocampinæ. Office USGP, editor. 1905.

17. Liu Z, Cao X, Liu Z, Cao X. Rondotia melanoleuca sp. nov., a new wild-mulberry silkworm from China (Lepidoptera, Bombycidae). Nota Lepidopterol. 2024;47: 49–56. doi:10.3897/nl.47.109920

18. Hossie TJ, Sherratt TN, Janzen DH, Hallwachs W. An eyespot that “blinks”: an open and shut case of eye mimicry in Eumorpha caterpillars (Lepidoptera: Sphingidae). J Nat Hist. 2013;47: 2915–2926. doi:10.1080/00222933.2013.791935

19. Sun W, Yu H, Shen Y, Banno Y, Xiang Z, Zhang Z. Phylogeny and evolutionary history of the silkworm. Sci China Life Sci. 2012;55: 483–496. doi:10.1007/s11427-012-4334-7

20. Yang S-Y, Han M-J, Kang L-F, Li Z-W, Shen Y-H, Zhang Z. Demographic history and gene flow during silkworm domestication. BMC Evol Biol. 2014;14: 185. doi:10.1186/s12862-014-0185-0

21. Han M, Ren J, Guo H, Tong X, Hu H, Lu K, et al. Mutation Rate and Spectrum of the Silkworm in Normal and Temperature Stress Conditions. Genes. 2023;14: 649. doi:10.3390/genes14030649

22. Xiang H, Liu X, Li M, Zhu Y, Wang L, Cui Y, et al. The evolutionary road from wild moth to domestic silkworm. Nat Ecol Evol. 2018;2: 1268–1279. doi:10.1038/s41559-018-0593-4

23. Kômoto N. Behavior of the larvae of wild mulberry silkworm Bombyx mandarina, domesticated silkworm B. mori and their hybrid. J Insect Biotechnol Sericology. 2017;86: 1_017-1_020. doi:10.11416/jibs.86.1_017

24. Lu K, Liang S, Han M, Wu C, Song J, Li C, et al. Flight Muscle and Wing Mechanical Properties are Involved in Flightlessness of the Domestic Silkmoth, Bombyx mori. Insects. 2020;11: 220. doi:10.3390/insects11040220

25. Fang S-M, Zhou Q-Z, Yu Q-Y, Zhang Z. Genetic and genomic analysis for cocoon yield traits in silkworm. Sci Rep. 2020;10: 5682. doi:10.1038/s41598-020-62507-9

26. Tomihara K, Andolfatto P, Kiuchi T. Allele specific knockouts reveal a role for apontic like in the evolutionary loss of larval melanin pigmentation in the domesticated silkworm, Bombyx mori. Insect Mol Biol. 2022;31: 701–710. doi:10.1111/imb.12797

27. Bisch-Knaden S, Daimon T, Shimada T, Hansson BS, Sachse S. Anatomical and functional analysis of domestication effects on the olfactory system of the silkmoth Bombyx mori. Proc R Soc B: Biol Sci. 2014;281: 20132582. doi:10.1098/rspb.2013.2582

28. Yu H-S, Shen Y-H, Yuan G-X, Hu Y-G, Xu H-E, Xiang Z-H, et al. Evidence of Selection at Melanin Synthesis Pathway Loci during Silkworm Domestication. Mol Biol Evol. 2011;28: 1785–1799. doi:10.1093/molbev/msr002

29. Orr HA. Testing Natural Selection vs. Genetic Drift in Phenotypic Evolution Using Quantitative Trait Locus Data. Genetics. 1998;149: 2099–2104. doi:10.1093/genetics/149.4.2099

30. Murat S, Hopfen C, McGregor AP. The function and evolution of Wnt genes in arthropods. Arthropod Struct Dev. 2010;39: 446–452. doi:10.1016/j.asd.2010.05.007

31. Loh KM, van Amerongen R, Nusse R. Generating Cellular Diversity and Spatial Form: Wnt Signaling and the Evolution of Multicellular Animals. Dev Cell. 2016;38: 643–655. doi:10.1016/j.devcel.2016.08.011

32. Wittkopp PJ, Haerum BK, Clark AG. Evolutionary changes in cis and trans gene regulation. Nature. 2004;430: 85–88. doi:10.1038/nature02698

33. Logan CY, Nusse R. THE WNT SIGNALING PATHWAY IN DEVELOPMENT AND DISEASE. Cell Dev Biol. 2004;20: 781–810. doi:10.1146/annurev.cellbio.20.010403.113126

34. Wiese KE, Nusse R, Amerongen R van. Wnt signalling: conquering complexity. Development. 2018;145: dev165902. doi:10.1242/dev.165902

35. Wodarz A, Nusse R. MECHANISMS OF WNT SIGNALING IN DEVELOPMENT. Cell Dev Biol. 1998;14: 59–88. doi:10.1146/annurev.cellbio.14.1.59

36. Hayat R, Manzoor M, Hussain A. Wnt signaling pathway: A comprehensive review. Cell Biol Int. 2022;46: 863–877. doi:10.1002/cbin.11797

37. Martin A, Papa R, Nadeau NJ, Hill RI, Counterman BA, Halder G, et al. Diversification of complex butterfly wing patterns by repeated regulatory evolution of a Wnt ligand. Proc Natl Acad Sci. 2012;109: 12632–12637. doi:10.1073/pnas.1204800109

38. Martin A, Reed RD. Wnt signaling underlies evolution and development of the butterfly wing pattern symmetry systems. Dev Biol. 2014;395: 367–378. doi:10.1016/j.ydbio.2014.08.031

39. Koshikawa S, Giorgianni MW, Vaccaro K, Kassner VA, Yoder JH, Werner T, et al. Gain of cis-regulatory activities underlies novel domains of wingless gene expression in Drosophila. Proc Natl Acad Sci. 2015;112: 7524–7529. doi:10.1073/pnas.1509022112

40. Bayala EX, VanKuren N, Massardo D, Kronforst MR. aristaless1 has a dual role in appendage formation and wing color specification during butterfly development. BMC Biol. 2023;21: 100. doi:10.1186/s12915-023-01601-6

41. Ando T, Fujiwara H, Kojima T. The pivotal role of aristaless in development and evolution of diverse antennal morphologies in moths and butterflies. BMC Evol Biol. 2018;18: 8. doi:10.1186/s12862-018-1124-2

42. Amerongen R van, Nusse R. Towards an integrated view of Wnt signaling in development. Development. 2009;136: 3205–3214. doi:10.1242/dev.033910

43. Gleason JE, Szyleyko EA, Eisenmann DM. Multiple redundant Wnt signaling components function in two processes during C. elegans vulval development. Dev Biol. 2006;298: 442–457. doi:10.1016/j.ydbio.2006.06.050

44. Quinlan R, Graf M, Mason I, Lumsden A, Kiecker C. Complex and dynamic patterns of Wnt pathway gene expression in the developing chick forebrain. Neural Dev. 2009;4: 35. doi:10.1186/1749-8104-4-35

45. Janson K, Cohen ED, Wilder EL. Expression of DWnt6, DWnt10, and DFz4 during Drosophila development. Mech Dev. 2001;103: 117–120. doi:10.1016/s0925-4773(01)00323-9

46. Bolognesi R, Beermann A, Farzana L, Wittkopp N, Lutz R, Balavoine G, et al. Tribolium Wnts: evidence for a larger repertoire in insects with overlapping expression patterns that suggest multiple redundant functions in embryogenesis. Dev Genes Evol. 2008;218: 193–202. doi:10.1007/s00427-007-0170-3

47. Harris RE, Setiawan L, Saul J, Hariharan IK. Localized epigenetic silencing of a damage-activated WNT enhancer limits regeneration in mature Drosophila imaginal discs. eLife. 2016;5: e11588. doi:10.7554/elife.11588

48. Andersson L, Purugganan M. Molecular genetic variation of animals and plants under domestication. Proc Natl Acad Sci. 2022;119: e2122150119. doi:10.1073/pnas.2122150119

49. Shapiro MD, Marks ME, Peichel CL, Blackman BK, Nereng KS, Jónsson B, et al. Genetic and developmental basis of evolutionary pelvic reduction in threespine sticklebacks. Nature. 2004;428: 717–723. doi:10.1038/nature02415

50. Liu Y, Ramos-Womack M, Han C, Reilly P, Brackett KL, Rogers W, et al. Changes throughout a Genetic Network Mask the Contribution of Hox Gene Evolution. Curr Biol. 2019;29: 2157-2166.e6. doi:10.1016/j.cub.2019.05.074

51. King EG, Long AD. The Beavis Effect in Next-Generation Mapping Panels in Drosophila melanogaster. G3: Genes, Genomes, Genet. 2017;7: 1643–1652. doi:10.1534/g3.117.041426

52. WD B. The power and deceit of QTL experiments: lessons from comparative QTL studies. Proceedings of the forty-ninth annual corn and sorghum industry research conference. 1994;250: 266.

53. Powell DL, Payne C, Banerjee SM, Keegan M, Bashkirova E, Cui R, et al. The Genetic Architecture of Variation in the Sexually Selected Sword Ornament and Its Evolution in Hybrid Populations. Curr Biol. 2021;31: 923-935.e11. doi:10.1016/j.cub.2020.12.049

54. Hayward LK, Sella G. Polygenic adaptation after a sudden change in environment. eLife. 2022;11: e66697. doi:10.7554/elife.66697

55. Navon D, Olearczyk N, Albertson RC. Genetic and developmental basis for fin shape variation in African cichlid fishes. Mol Ecol. 2017;26: 291–303. doi:10.1111/mec.13905

56. Yamaguchi J, Banno Y, Mita K, Yamamoto K, Ando T, Fujiwara H. Periodic Wnt1 expression in response to ecdysteroid generates twin-spot markings on caterpillars. Nat Commun. 2013;4: 1857. doi:10.1038/ncomms2778

57. Edayoshi M, Yamaguchi J, Fujiwara H. Protruding Structures on Caterpillars Are Controlled by Ectopic Wnt1 Expression. PLoS ONE. 2015;10: e0121736. doi:10.1371/journal.pone.0121736

58. Sihvonen P, Murillo-Ramos L, Wahlberg N, Hausmann A, Zilli A, Ochse M, et al. Insect taxonomy can be difficult: a noctuid moth (Agaristinae: Aletopus imperialis) and a geometrid moth (Sterrhinae: Cartaletis dargei) combined into a cryptic species complex in eastern Africa (Lepidoptera). PeerJ. 2021;9: e11613. doi:10.7717/peerj.11613

59. Kitching IJ, Rougerie R, Zwick A, Hamilton CA, Laurent RAS, Naumann S, et al. A global checklist of the Bombycoidea (Insecta: Lepidoptera). Biodivers Data J. 2018;6: e22236. doi:10.3897/bdj.6.e22236

60. Espeland M, Breinholt J, Willmott KR, Warren AD, Vila R, Toussaint EFA, et al. A Comprehensive and Dated Phylogenomic Analysis of Butterflies. Curr Biol. 2018;28: 770-778.e5. doi:10.1016/j.cub.2018.01.061

61. Kawahara AY, Plotkin D, Espeland M, Meusemann K, Toussaint EFA, Donath A, et al. Phylogenomics reveals the evolutionary timing and pattern of butterflies and moths. Proc Natl Acad Sci United States Am. 2019;116: 22657–22663. doi:10.1073/pnas.1907847116

62. Hamilton CA, Laurent RAS, Dexter K, Kitching IJ, Breinholt JW, Zwick A, et al. Phylogenomics resolves major relationships and reveals significant diversification rate shifts in the evolution of silk moths and relatives. BMC Evol Biol. 2019;19: 182. doi:10.1186/s12862-019-1505-1

63. Deng M, Liao C, Chen Q, Huang G, Wang X. Phylogenetic relationships among Bombycinae (Lepidoptera, Bombycoidea, and Bombycidae) based on mitochondrial genomes. Arch Insect Biochem Physiol. 2022;111: e21889. doi:10.1002/arch.21889

64. Daimon T, Yago M, Hsu Y-F, Fujii T, Nakajima Y, Kokusho R, et al. Molecular phylogeny, laboratory rearing, and karyotype of the bombycid moth, Trilocha varians. J Insect Sci. 2012;12: 49. doi:10.1673/031.012.4901

65. Schneider CA, Rasband WS, Eliceiri KW. NIH Image to ImageJ: 25 years of image analysis. Nat methods. 2012;9: 671–5. doi:10.1038/nmeth.2089

66. Andolfatto P, Davison D, Erezyilmaz D, Hu TT, Mast J, Sunayama-Morita T, et al. Multiplexed shotgun genotyping for rapid and efficient genetic mapping. Genome Res. 2011;21: 610–617. doi:10.1101/gr.115402.110

67. Picelli S, Björklund ÅK, Reinius B, Sagasser S, Winberg G, Sandberg R. Tn5 transposase and tagmentation procedures for massively scaled sequencing projects. Genome Res. 2014;24: 2033–2040. doi:10.1101/gr.177881.114

68. Kawamoto M, Jouraku A, Toyoda A, Yokoi K, Minakuchi Y, Katsuma S, et al. High-quality genome assembly of the silkworm, Bombyx mori. Insect Biochem Mol Biol. 2019;107: 53–62. doi:10.1016/j.ibmb.2019.02.002

69. Li H. Aligning sequence reads, clone sequences and assembly contigs with BWA-MEM. arXiv. 2013. doi:10.48550/arxiv.1303.3997

70. Danecek P, Bonfield JK, Liddle J, Marshall J, Ohan V, Pollard MO, et al. Twelve years of SAMtools and BCFtools. GigaScience. 2021;10: giab008. doi:10.1093/gigascience/giab008

71. Broman KW, Wu H, Sen Ś, Churchill GA. R/qtl: QTL mapping in experimental crosses. Bioinformatics. 2003;19: 889–890. doi:10.1093/bioinformatics/btg112

72. Haley CS, Knott SA. A simple regression method for mapping quantitative trait loci in line crosses using flanking markers. Heredity. 1992;69: 315–324. doi:10.1038/hdy.1992.131

73. Churchill GA, Doerge RW. Empirical threshold values for quantitative trait mapping. Genetics. 1994;138: 963–971. doi:10.1093/genetics/138.3.963

74. Dupuis J, Siegmund D. Statistical Methods for Mapping Quantitative Trait Loci From a Dense Set of Markers. Genetics. 1999;151: 373–386. doi:10.1093/genetics/151.1.373

75. Dobin A, Davis CA, Schlesinger F, Drenkow J, Zaleski C, Jha S, et al. STAR: ultrafast universal RNA-seq aligner. Bioinformatics. 2012;29: 15–21. doi:10.1093/bioinformatics/bts635

76. Love MI, Huber W, Anders S. Moderated estimation of fold change and dispersion for RNA-seq data with DESeq2. Genome Biol. 2014;15: 550. doi:10.1186/s13059-014-0550-8

77. Hinrichs AS, Karolchik D, Baertsch R, Barber GP, Bejerano G, Clawson H, et al. The UCSC Genome Browser Database: update 2006. Nucleic acids Res. 2005;34: D590-8. doi:10.1093/nar/gkj144

78. Slater GSC, Birney E. Automated generation of heuristics for biological sequence comparison. BMC Bioinform. 2005;6: 31–31. doi:10.1186/1471-2105-6-31

79. Edgar RC. MUSCLE: multiple sequence alignment with high accuracy and high throughput. Nucleic acids Res. 2004;32: 1792–7. doi:10.1093/nar/gkh340

80. Gouy M, Tannier E, Comte N, Parsons DP. Multiple Sequence Alignment, Methods and Protocols. Methods Mol Biol. 2020;2231: 241–260. doi:10.1007/978-1-0716-1036-7_15

81. Fujii T, Kiuchi T, Daimon T, Ito K, Katsuma S, Shimada T, et al. Development of interspecific semiconsomic strains between the domesticated silkworm, Bombyx mori and the wild silkworm, B. mandarina. J Insect Biotechnol Sericology. 2021;90: 2_033-2_040. doi:10.11416/jibs.90.2_033

82. Kogure M. The Influence Of Light And Temperature On Certain Characters Of The Silkworm, Bombyx Mori. J Fac Agric, Kyushu Univ. 1933;4: 1–93. doi:10.5109/22568

83. Yamaguchi J, Mizoguchi T, Fujiwara H. siRNAs Induce Efficient RNAi Response in Bombyx mori Embryos. PLoS ONE. 2011;6: e25469. doi:10.1371/journal.pone.0025469

84. Truett GE, Heeger P, Mynatt RL, Truett AA, Walker JA, Warman ML. Preparation of PCR-Quality Mouse Genomic DNA with Hot Sodium Hydroxide and Tris (HotSHOT). BioTechniques. 2000;29: 52–54. doi:10.2144/00291bm09

85. Ota S, Hisano Y, Muraki M, Hoshijima K, Dahlem TJ, Grunwald DJ, et al. Efficient identification of TALEN□mediated genome modifications using heteroduplex mobility assays. Genes Cells. 2013;18: 450–458. doi:10.1111/gtc.12050

86. Ansai S, Inohaya K, Yoshiura Y, Schartl M, Uemura N, Takahashi R, et al. Design, evaluation, and screening methods for efficient targeted mutagenesis with transcription activator□like effector nucleases in medaka. Dev, Growth Differ. 2014;56: 98–107. doi:10.1111/dgd.12104

87. Gutin. THE GENETICS OF MORPHOLOGICAL EVOLUTION IN SILKWORMS (BOMBYCIDAE: BOMBYX). Princeton, NJ□: Princeton University. 2019.

88. Lin R-J, Braby MF, Hsu Y-F. The Immature Stages, Biology, and Phylogenetic Relationships of Rotunda rotundapex (Lepidoptera: Bombycidae). J Insect Sci. 2019;19: 19. doi:10.1093/jisesa/iez025

89. Takeda S. Encyclopedia of Insects (Second Edition). B. 2009; 117–119. doi:10.1016/b978-0-12-374144-8.00040-0

Figure legends

Main Figures

Fig 1. Evolutionary diversification of Lepidopteran larval appendages. (A) Representative morphological diversity among Lepidopteran caterpillars. Phylogenetic relationships are indicated by the cladogram and family names for each representative species are indicated. *Bombyx* belongs to the Bombicidae (highlighted in red). (B) Representative caudal horn diversity among species in the Bombicidae family. Shown are the posterior larval segments for each species; the cladogram depicts their phylogenetic relationships [58–64,88]. A full list of photo credits is provided in **S1 Table**. Data can be found in DOI 10.5281/zenodo.17833042.

Fig 2. QTL analyses for caudal horn length. (A) Distributions of caudal horn lengths (CH) in *B. mori* p50T and *B. mandarina* (Sakado) parental species and hybrids. F1 hybrids are the progeny of p50T females × Sakado males; BC1 are the progeny of p50T females and F1 males; F2 are the progeny of F1 hybrids generated by crossing *B. mori* p50T males and *B. mandarina* Sakado females. The inset shows representative parental phenotypes (see also **S1 Fig**). Red dashed lines represent the length measurements for these individuals. Photographs by Kenta Tomihara. (B) QTL LOD profile plots for caudal horn length based on the BC1 mapping panel. LOD is shown in black with a red dashed line indicating the estimated significance threshold (3.02) determined by 1000

phenotype permutations. Red arrows indicate significant QTL peaks. (C) Caudal horn length distributions of BC1 individuals based on marker genotypes immediately under the three highest LOD peaks on chromosomes 4, 5, and 21. Caudal horn lengths are adjusted for larval weight and sex. The last panel shows caudal horn distributions of BC1 individuals whose genotypes are jointly homozygous *B. mori* or jointly heterozygous at all three QTL. Effect sizes are indicated in blue and represent the change in length as a proportion of the mean length difference between parental species; t-test p-values are indicated as follows: $p < 0.01$ = **, $p < .0005$ = ***. (D) Annotation of the chromosome 4 QTL interval. Boxes indicate annotated genes within the 1.5 LOD interval (delimited by dashed lines) estimated in the BC1 QTL analysis (**S4 Table**). Wnt family genes are colored in orange. Coordinates are in Megabase pairs (Mbp). Data can be found in DOI 10.5281/zenodo.17833042.

Fig 3. Cis-regulatory divergence underlies species- and tissue-specific *Wnt1* and *Wnt6* expression patterns during larval development. (A) Schematic of the sampling scheme for gene expression analyses. Total RNA was extracted from caudal horn (CH, segment A8) and non-horn tissue of the eighth abdominal segment (A8) for RNA-seq (**S6A Fig**) and targeted ASE (**Fig 3B and S6B Fig**). Total RNA from the integument of segments A7 and A8 was extracted for RNA-seq (**S6A Fig**) and the temporal expression analysis (**Fig 3C and S6C Fig**). Diagram based on Takeda (2009). [89] (B) Allele-specific expression patterns in the caudal horn of *B. mori* (p50T) × *B. mandarina* (Sakado) F1 hybrids of L5 (final) instar caterpillars. Plotted for each gene in the QTL interval (in the same order, left to right), is the

log2(fold-difference) in the average *B. mori* and *B. mandarina* allele counts for the caudal horn portion of segment A8. Values larger than 0 indicate higher expression of the *B. mandarina* allele and whiskers represent two standard errors (corresponding to 95% confidence intervals among biological replicates). "CH" shows the caudal horn tissue and "A8" the non-horn tissue portion (Fig3A). A corresponding analysis of L1 (first) instar caterpillars is shown in **S6B Fig**. Significance of ASE differences between the caudal and non-caudal portions of segment A8 were evaluated using the inverted beta-binomial test (ibb) test for paired count data and significant differences are indicated with asterisks (Bonferroni corrected, **S6 Table**). (C) Temporally-elevated expression of *Wnt1* and *Wnt6* in segment A8 of *B. mandarina*. Temporal expression of *Wnt1* and *Wnt6* in the integument tissue of segment A8 during the transition between fourth and fifth instar stages of *B. mori* and *B. mandarina* caterpillar development. A corresponding analysis of segment A7 is shown in **S6C Fig**. Relative *Wnt1* and *Wnt6* expression levels (setting *B. mori* A8 at day 0 of 4th instar = 1) were normalized to those of *ribosomal protein 49* (*rp49*). Whiskers represent two standard errors among replicates. Data can be found in DOI 10.5281/zenodo.17833042.

Fig 4. *Wnt1* and *Wnt6* CRISPR/Cas9-mediated *B. mandarina*-allele-specific knockouts significantly reduce caudal horn length. (A) Distributions of caudal horn lengths for larvae at day 0 of the fifth instar (L5). Diagrams to the left indicate the genotypes of the strains being compared (Chr4=chromosome 4; GB=genomic background). Blue corresponds to the p50T *B. mori* background; and red to the *B. mandarina* Sakado background. $chr4^{mand \cdot Wnt1}/chr4^{mori}$ and $chr4^{mand \cdot Wnt6}/chr4^{mori}$

correspond to CRISPR/Cas9-mediated *B. mandarina*-allele-specific knockouts of *Wnt1* and *Wnt6*, respectively. White points indicate individual caterpillar horn lengths, corrected for caterpillar weight (a proxy for size). Black points and whiskers correspond to means and standard errors. Letters on the right indicate groups that differ significantly in caudal horn length based on a one-way ANOVA followed by Tukey's HSD test (family-wise confidence level = 95%). A significant positive allometric relationship was observed between body weight and caudal horn length (ANCOVA: effect of weight, $p = 2.9 \times 10^{-1}$), with a significantly steeper slope in *B. mandarina* than in *B. mori* (interaction term, $p = 0.016$), see **S1 Fig**. (B) Conceptual representation of relative *Wnt1* and *Wnt6* transcriptional abundances for each genotype. Expression results (**Fig 3**) indicate that *Wnt1* and *Wnt6* have elevated transcript abundance in caudal horn tissue of stage L5 *B. mandarina* caterpillars. Knock-outs of the *B. mandarina* allele are expected to decrease (but not eliminate) expression of *Wnt1* or *Wnt6* relative to all other genotypes in the entire animal. Data can be found in DOI 10.5281/zenodo.17833042.

Supplementary Figures

S1 Fig. Measurement of caudal horn length variation. (A) Images of L5 larval caudal horns were marked at three locations (colored points) using MATLAB or ImageJ. Two purple points are laid to mark the base of the caudal horn, corresponding to $X_{1,2}$,$Y_{1,2}$ (see Methods: Rearing and Phenotyping), and the black point marks the vertex X_3,Y_3. The height of the triangle is then added to the distance between the black point and the

blue point X_4,Y_4 located at the tip of the caudal horn. Photographs by Kenta Tomihara. (B) Caudal horn (CH) length measurements across various strains of *B. mori* and *B. mandarina* Sakado. The *B. mori* strain used in this study is p50T. Values were not adjusted for weight or sex. (C) Neonate (day 0 of first instar) larvae of *B. mori* (left) and *B. mandarina* (right). Red arrows indicate the caudal horns. Scale bars = 1 mm. (D) Caudal horn (CH) length and caterpillar weight relationship for *B. mori* (p50T) and *B. mandarina* (Sakado) at L5 stage. Values were not adjusted for weight or sex. Data can be found in DOI 10.5281/zenodo.17833042.

S2 Fig. Schematic of the cross design for the BC1 and F2 mapping panels. (A) The BC1 mapping panel. *B. mandarina* Sakado (Bmand) males were crossed to *B. mori* (Bmori) p50T females to create F1 males. F1 males were then backcrossed to *B. mori* p50T to produce BC1 progeny. Note that the W chromosome of BC1 females (red) is derived from *B. mori* p50T. The large X indicates meiotic crossing over in F1 males. (B) The F2 mapping panel. *B. mori* p50T (Bmori) males were crossed to a *B. mandarina* (Bmand) Sakado females to create F1 males. F1 males and females were crossed to produce F2 progeny. Note that the W chromosome of F2 females (black) is derived from *B. mandarina* Sakado. The large X indicates meiotic crossing over in F1 males. Data can be found in DOI 10.5281/zenodo.17833042.

S3 Fig. F2 QTL analysis and estimated QTL effect sizes. (A) Caudal horn (CH) length distributions of BC1 individuals based for markers corresponding to maximum LOD peaks for QTLs on chromosomes 7, 9, 10, 25, and 26. Caudal horn

length was adjusted for larval sex and weight. Effect sizes (in blue) are the % mean length difference between heterozygous (mori:mand) and homozygous *B. mori* (mori:mori) genotype, normalized by the mean length difference between the parental species. (B) F2 QTL LOD profile for caudal horn length. LOD is shown in blue with the red dashed line indicating the LOD significance threshold of 3.62 determined by 1000 permutations. (C) Superposition of BC1 (black) and F2 (blue) LOD profiles for Chr4. The vertical line and red triangle indicate the max LOD position in BC1. LOD significance threshold for BC1 is 3.02, and F2 is 3.62. (D) Caudal horn length distributions of F2 individuals based on marker genotypes immediately under the LOD peak at chromosome 4. Lengths are adjusted for larval weight. Effect sizes are indicated in blue and represent the change in length as a proportion of the mean length difference between parental species; t-test p-values are indicated as follows: $p < 0.01$ = **, $p < .0005$ = ***. Data can be found in DOI 10.5281/zenodo.17833042.

S4 Fig. Analysis of consomic and semi-consomic Chr4 introgression strains. (A) Schematic diagram showing genome-wide ancestry of semi-consomic (T04) and consomic (CT04) strains. The semiconsomic strain T04 segregates for a *B. mandarina* (Sakado) derived chromosome 4 in an otherwise *B. mori* (p50T) genomic background [81]. In contrast, the consomic CT04 strain is homozygous for the *B. mandarina* (Sakado) derived chromosome 4 in the same *B. mori* (p50T) background. Individual caterpillars were genotyped to identify those with one copy ($chr4^{mand}/chr4^{mori}$) versus zero copies ($chr4^{mori}/chr4^{mori}$) of *B. mandarina* chromosome 4 (see Methods). The mean caudal horn length of $chr4^{mori}/chr4^{mori}$ individuals is 15% shorter than

chr4^{mand}/chr4^{mori} and chr4^{mand}/chr4^{mand} individuals (**S4 Fig**), which is consistent with the direction, dominance and effect size estimated for the chromosome 4 QTL. (B) Caudal horn length distributions among Chr4 genotypes. Caudal horn length was adjusted for larval weight and sex. Effect sizes are indicated in blue and represent the change in length as a proportion of the mean length difference between parental species. A significant difference in corrected caudal horn length was observed between mori:mori and mori:mandarina T04 individuals (t-test, p = 1.0 × 10••; means ± SE: 1.01 ± 0.04 mm vs. 1.44 ± 0.03 mm, respectively). Data can be found in DOI 10.5281/zenodo.17833042.

S5 Fig. Caudal horn length is unlikely to have a highly polygenic architecture. BC1 data shown in panels A, B and C; F2 data shown in panels D, E and F. (A) The correlation between caudal horn length and genome-wide ancestry for BC1 (Pearson's • = 0.32, p= 1.3e-17). Caudal horn length was adjusted for larval weight and sex. (B) The correlation between caudal horn length and genome-wide ancestry excluding chromosomes with significant QTLs for BC1 (Pearson's • = 0.05, p= 0.23). Caudal horn length was adjusted for larval weight and sex. (C) The estimated effect sizes of *B. mandarina* ancestry on each BC_1 chromosome using a BIC model selection approach to select the minimal set of chromosomes that explain caudal horn length. Sex and weight were included as covariates. Bolded chromosomes are chromosomes carrying caudal horn length QTLs. Adjusted p-values are shown for significant chromosomes observed in the model. (D) The correlation between caudal horn length and genome-wide ancestry for F2 (Pearson's • = 0.45, p= 1.76e-17). Caudal horn length was adjusted for larval weight. (E) The correlation between caudal horn length and

genome-wide ancestry excluding chromosomes with significant QTLs for F2 (Pearson's • = 0.27, p= 6.4e-7). Caudal horn length was adjusted for larval weight. (F) The estimated effect sizes of *B. mandarina* ancestry on each F2 chromosome using a BIC model selection approach to select the minimal set of chromosomes that explain caudal horn length. Sex and weight were included as covariates. Bolded chromosomes are chromosomes carrying caudal horn length QTLs. Bonferroni-corrected p-values are shown for significant chromosomes observed in the model. Data can be found in DOI 10.5281/zenodo.17833042.

S6 Fig. Gene expression analysis of parental species and F1 hybrids. (A) Normalized RNAseq counts from second instar larvae (L2) for non-caudal (A7) and caudal (A8) segments of *B. mori* (Bmori) and *B. mandarina* (Bmand). The asterisk indicates a significant species*segment difference for *Wnt6* (adjusted p-value = 0.023). Numbered genes exclude the prefix "KWMTBOMO", see **S4 Table**. (B) Allele-specific expression of caudal horn (CH) and non-caudal horn (A8) portions of the A8 segment for L1 (first) instar caterpillars (see **Fig 3A**). The fold-difference between *B. mori* (Bmori) and *B. mandarina* (Bmand) alleles is estimated as log2 of the ratio of the averages among the four replicate pools of 10 individuals. Positive values indicate higher expression of the *B. mandarina* allele. (C) Temporal expression of *Wnt1* and *Wnt6* in the A7 ("non-caudal") segment of *B. mori* and *B. mandarina* throughout fourth instar instar (setting *B. mori* A8 at day 0 of 4th instar = 1). The relative mRNA levels are normalized to that of *ribosomal protein 49* (*rp49*). Error bars represent two standard errors. For caudal segment analysis refer to **Fig 3D**. Data can be found in DOI 10.5281/zenodo.17833042.

S7 Fig. Design of CRISPR/Cas9-mediated allele-specific knockouts & breeding and screening strategy. Gene structures and inset alignments of (A) *Wnt1* and (B) *Wnt6* with selected crRNA target sites whose PAM sequences are only present in *B. mandarina*. The target sequences are underlined, and the PAM sequences are shown in bold letters. *B. mandarina* specific SNPs are highlighted with green shadings. Deletions introduced by CRISPR/Cas9 system are indicated by dashes. (C) Breeding and screening strategy used to generate and phenotype *Wnt* knockouts. T04 individuals (G0) were injected with Cas9-crRNA-tracrRNA complex targeting *Wnt1* or *Wnt6* and crossed to *B. mori* (p50T). G1 progeny were genotyped by heteroduplex mobility assay and Sanger sequenced to identify frameshift mutations. Selected G1 mutants were crossed to *B. mori* to produce G2 larvae. G2s were phenotyped for body weight and caudal horn length, then genotyped using PCR. Because chromosomes other than Chr4 were randomly inherited, off-target effects were assumed to have minimal phenotypic impact. Notably, G2 individuals homozygous for the *B. mori* allele at Chr4 (chr4 mori:mori) did not display aberrant phenotypes. (D) Chr4 genotype, genetic background (GB), and representative phenotype images for G2 individuals. Diagrams to the left indicate the genotypes of the strains being compared (Chr4=chromosome 4; GB=genomic background). Blue corresponds to the p50T *B. mori* background; and red to the *B. mandarina* Sakado background. $chr4^{mand \cdot Wnt1}/chr4^{mori}$ and $chr4^{mand \cdot Wnt6}/chr4^{mori}$ correspond to CRISPR/Cas9-mediated *B. mandarina*-allele-specific knockouts of *Wnt1* and *Wnt6*, respectively. Representative lateral views of the caudal

horn are shown for each class (scale bar, 1 mm). Photographs by Kenta Tomihara. Data can be found in DOI 10.5281/zenodo.17833042.

Supplementary Tables

Table S1. Licensing and attribution details for photographs used in Fig 1.

Table S2. Summary of BC1 QTL analysis.

Table S3. Summary of F2 QTL analysis.

Table S4. Annotated genes within the BC1 chromosome 4 QTL interval.

Table S5. Differential expression analysis between B. mori and B. mandarina in caudal and non-caudal segments of second instar larvae for genes in the Chr4 QTL interval.

Table S6. Comparison of allele-specific expression in caudal horn (CH) and non-horn A8 tissue.

Table S7. Examples of major upstream regulator genes with cis-regulatory changes that underlie trait differences between closely related or domesticated animal species.

Table S8. Primer pairs used for Allele Specific Expression (ASE) analysis in F1 hybrids.

Table S9. Primers used for RT-qPCR assays.

Table S10. RNA oligo and PCR primer list used in CRISPR/Cas9-mediated allele-specific knockouts.

Supplementary Data

Supplemental Data 1. Distribution of caudal horn length in *B. mori*, *B. mandarina*, and hybrids (Figure 2A).

Supplemental Data 2. Tissue-specific expression divergence between B. mori and B. mandarina in 2nd instar (L2) larvae.

Supplemental Data 3. Raw read counts for *B. mori* and *B. mandarina* alleles without allowing for mismatches.

Supplemental Data 4. Mean values plotted in figures for easy cross referencing.

Supplemental Data 5. Metadata for ASE experiment (Fig3B).

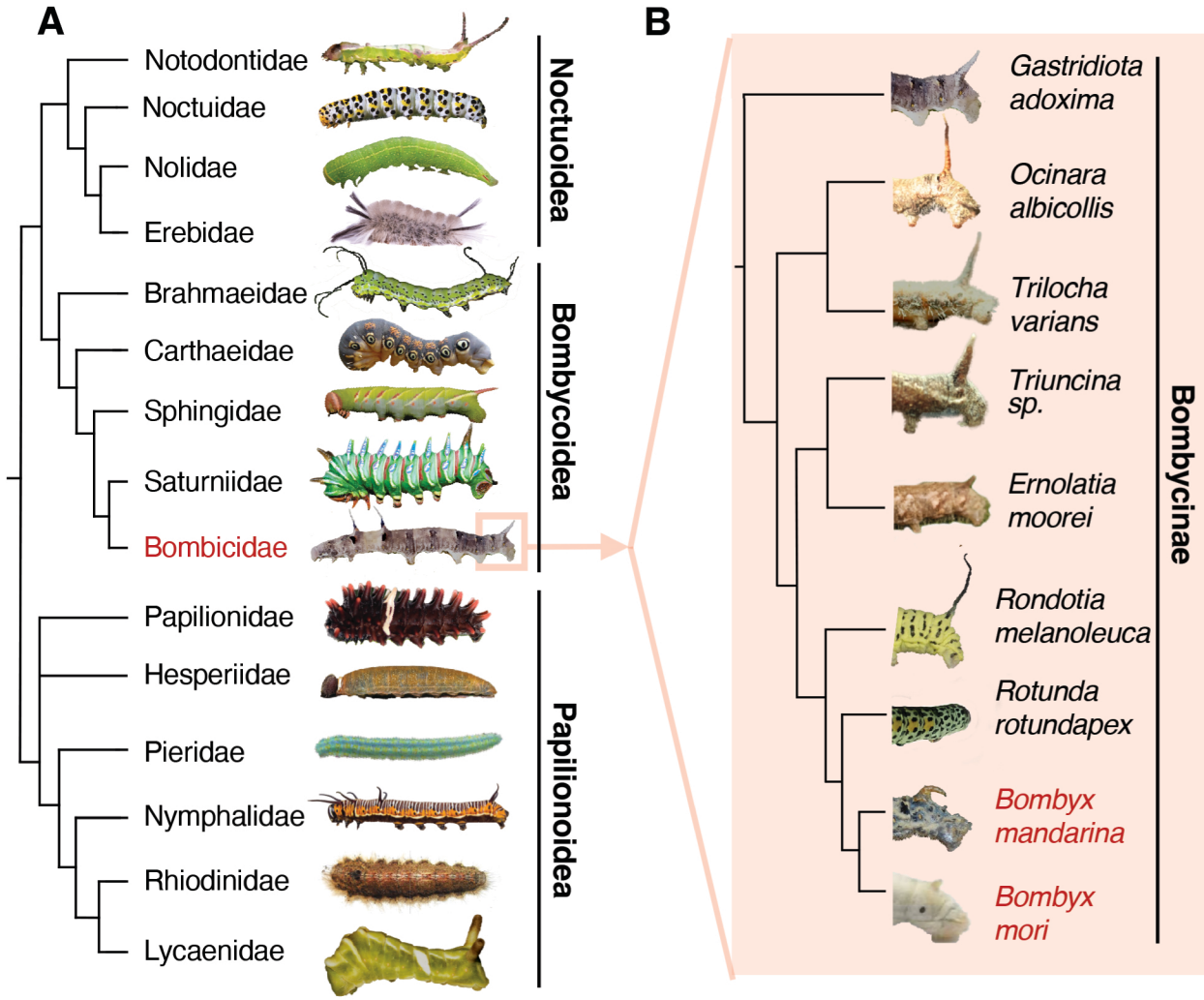
A
Notodontidae
Noctuidae
Nolidae
Erebidae
Brahmaeidae
Carthaeidae
Sphingidae
Saturniidae
Bombicidae
Papilionidae
Hesperiidae
Pieridae
Nymphalidae
Rhiodinidae
Lycaenidae
Noctuoidea
Bombycoidea
Papilionoidea
B
Gastridiota adoxima
Ocinara albicollis
Trilocha varians
Triuncina sp.
Ernolatia moorei
Rondotia melanoleuca
Rotunda rotundapex
Bombyx mandarina
Bombyx mori
Bombycinae

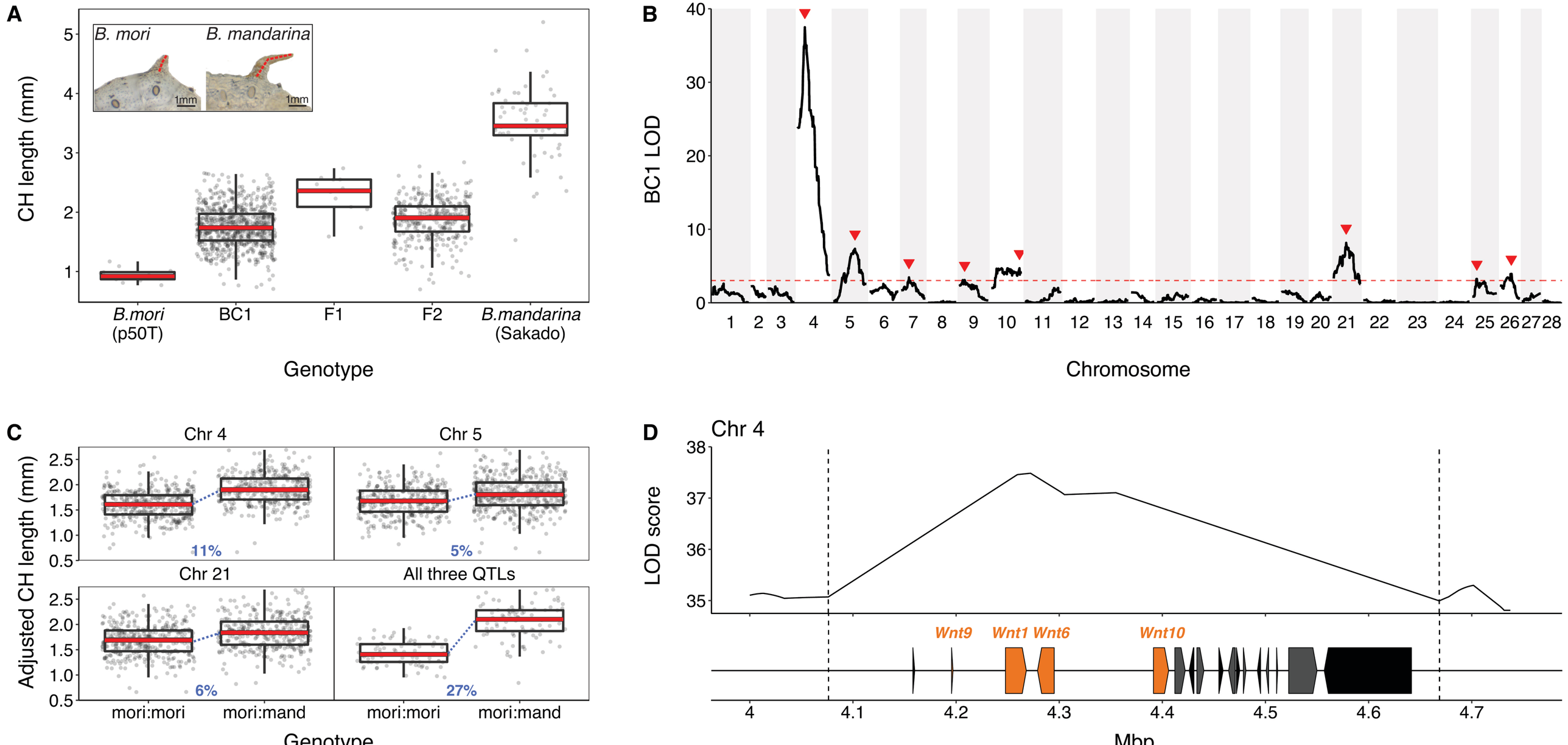
A
B. mori
B. mandarina
1mm
1mm
CH length (mm)
B.mori (p50T)
BC1
F1
F2
B.mandarina (Sakado)
Genotype
B
BC1 LOD
Chromosome
C
Chr 4
Chr 5
Chr 21
All three QTLs
11%
5%
6%
27%
Adjusted CH length (mm)
mori:mori
mori:mand
Genotype
D
Chr 4
LOD score
Wnt9
Wnt1
Wnt6
Wnt10
Mbp

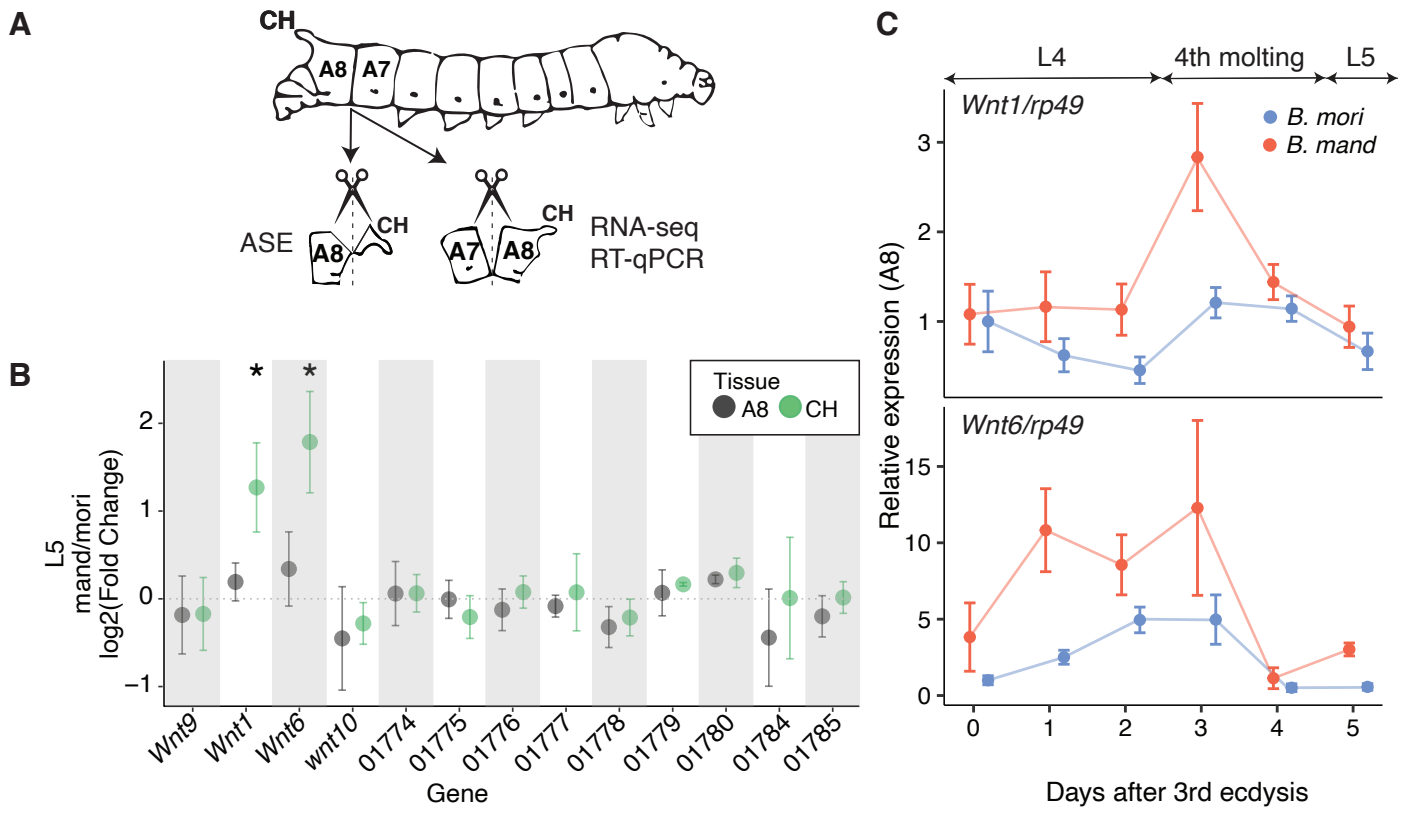
A
CH
A8
A7
ASE
CH
A8
A7
A8
CH
RNA-seq
RT-qPCR
B
Tissue
A8
CH
L5
mand/mori
log2(Fold Change)
Wnt9
Wnt1
Wnt6
wnt10
01774
01775
01776
01777
01778
01779
01780
01784
01785
Gene
C
L4
4th molting
L5
Wnt1/rp49
B. mori
B. mand
Wnt6/rp49
Relative expression (A8)
Days after 3rd ecdysis

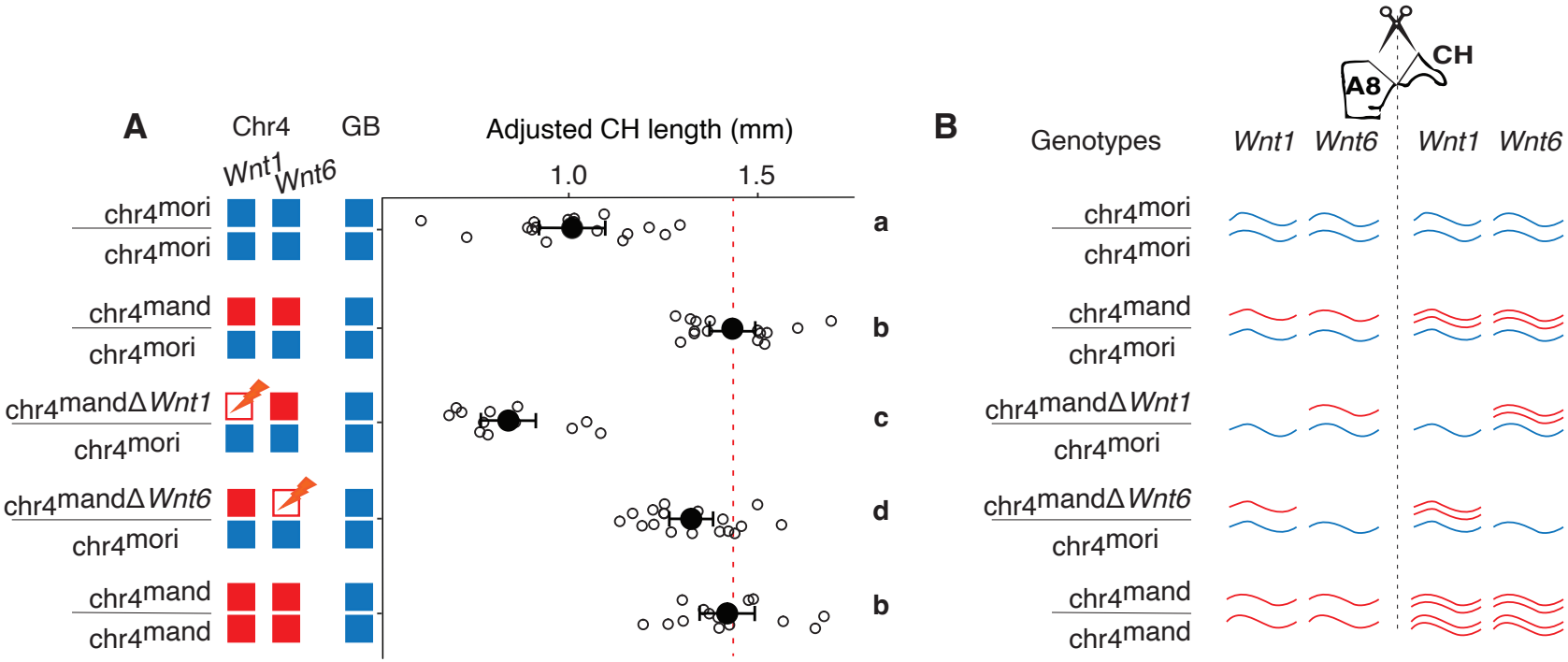
A
Chr4
GB
Wnt1
Wnt6
Adjusted CH length (mm)
1.0
1.5
chr4mori
chr4mori
chr4mand
chr4mori
chr4mandΔWnt1
chr4mori
chr4mandΔWnt6
chr4mori
chr4mand
chr4mand
a
b
c
d
b
B
CH
A8
Genotypes
Wnt1
Wnt6
Wnt1
Wnt6
chr4mori
chr4mori
chr4mand
chr4mori
chr4mandΔWnt1
chr4mori
chr4mandΔWnt6
chr4mori
chr4mand
chr4mand

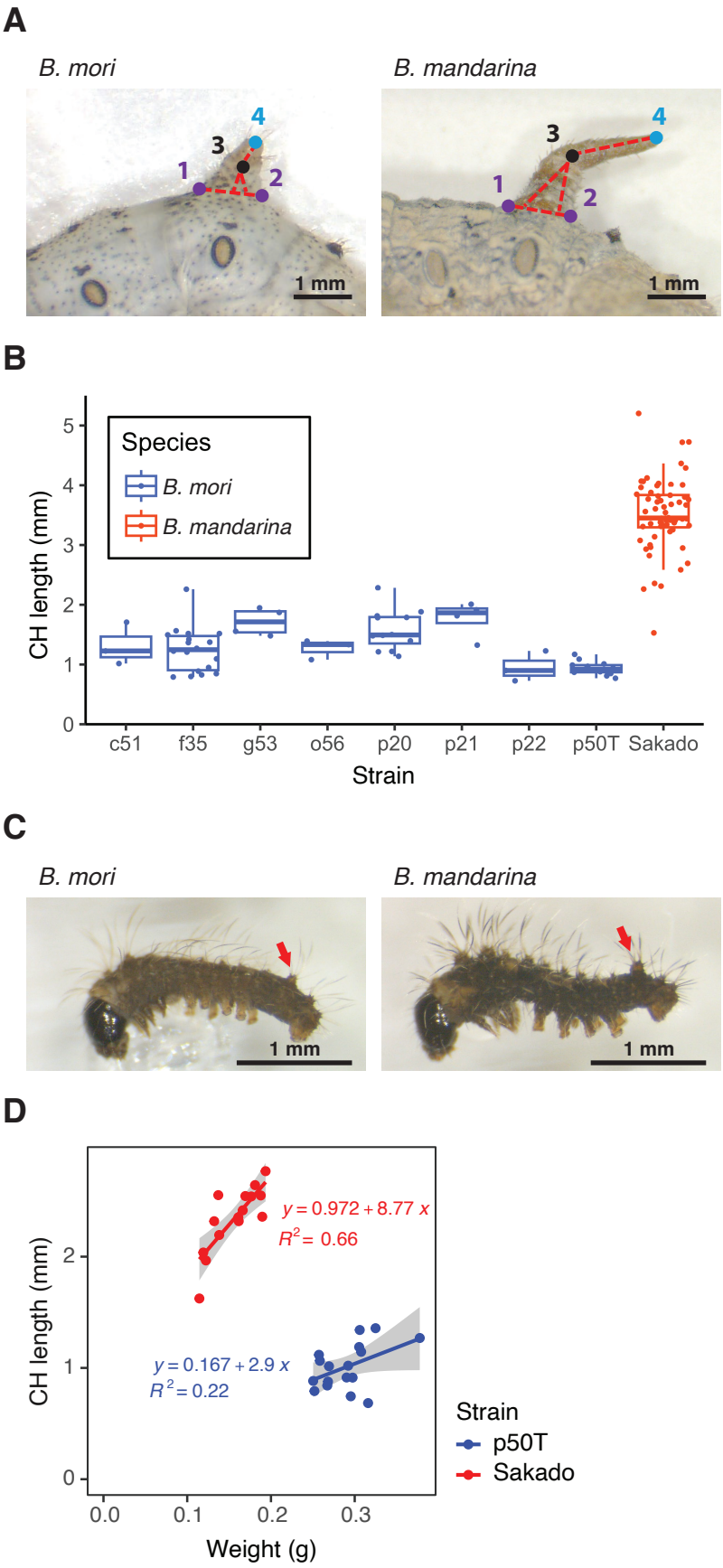
A
B. mori
B. mandarina
1
2
3
4
1 mm
B
Species
B. mori
B. mandarina
CH length (mm)
0
1
2
3
4
5
c51
f35
g53
o56
p20
p21
p22
p50T
Sakado
Strain
C
B. mori
B. mandarina
1 mm
D
y = 0.972 + 8.77 x
R2 = 0.66
y = 0.167 + 2.9 x
R2 = 0.22
CH length (mm)
0
1
2
0.0
0.1
0.2
0.3
Weight (g)
Strain
p50T
Sakado

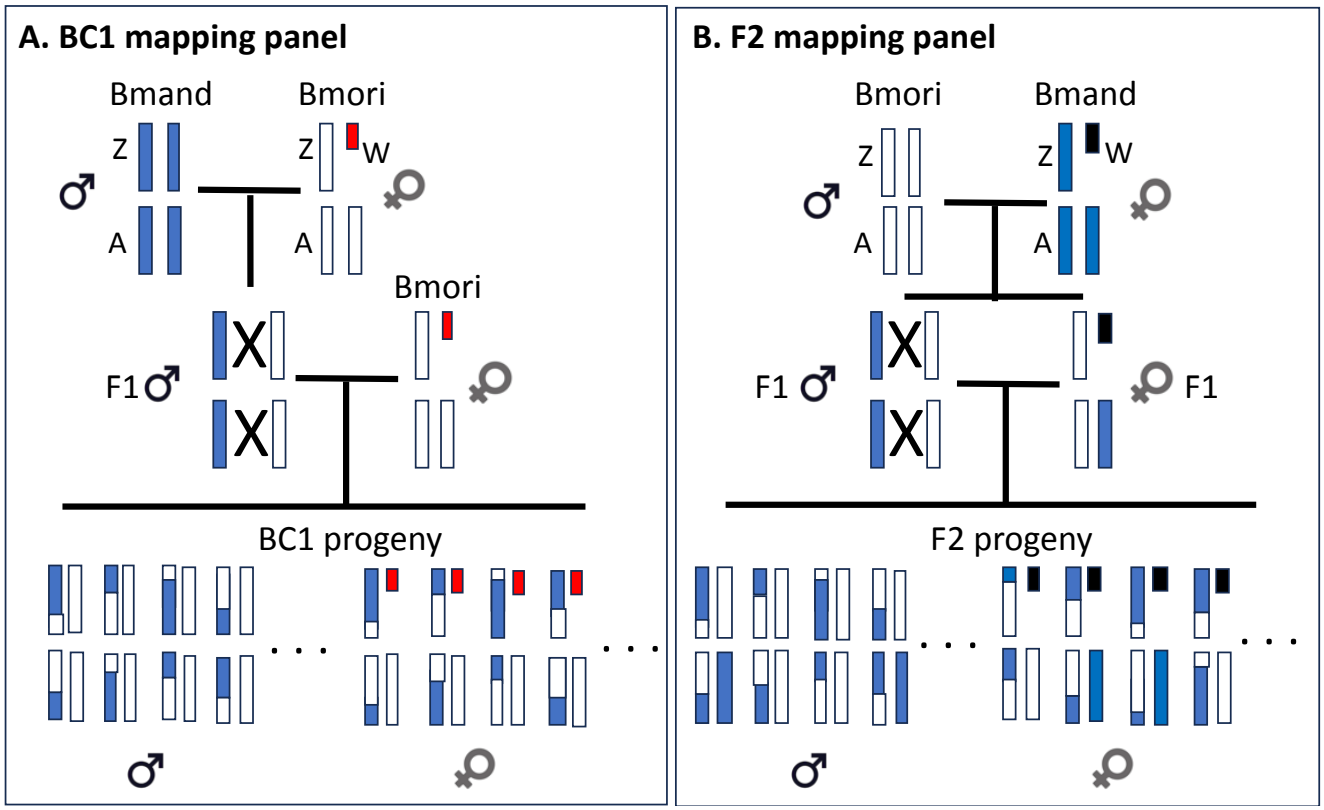
A. BC1 mapping panel
Bmand
Bmori
Z
Z
W
A
A
Bmori
F1
BC1 progeny
B. F2 mapping panel
Bmori
Bmand
Z
Z
W
A
A
F1
F1
F2 progeny

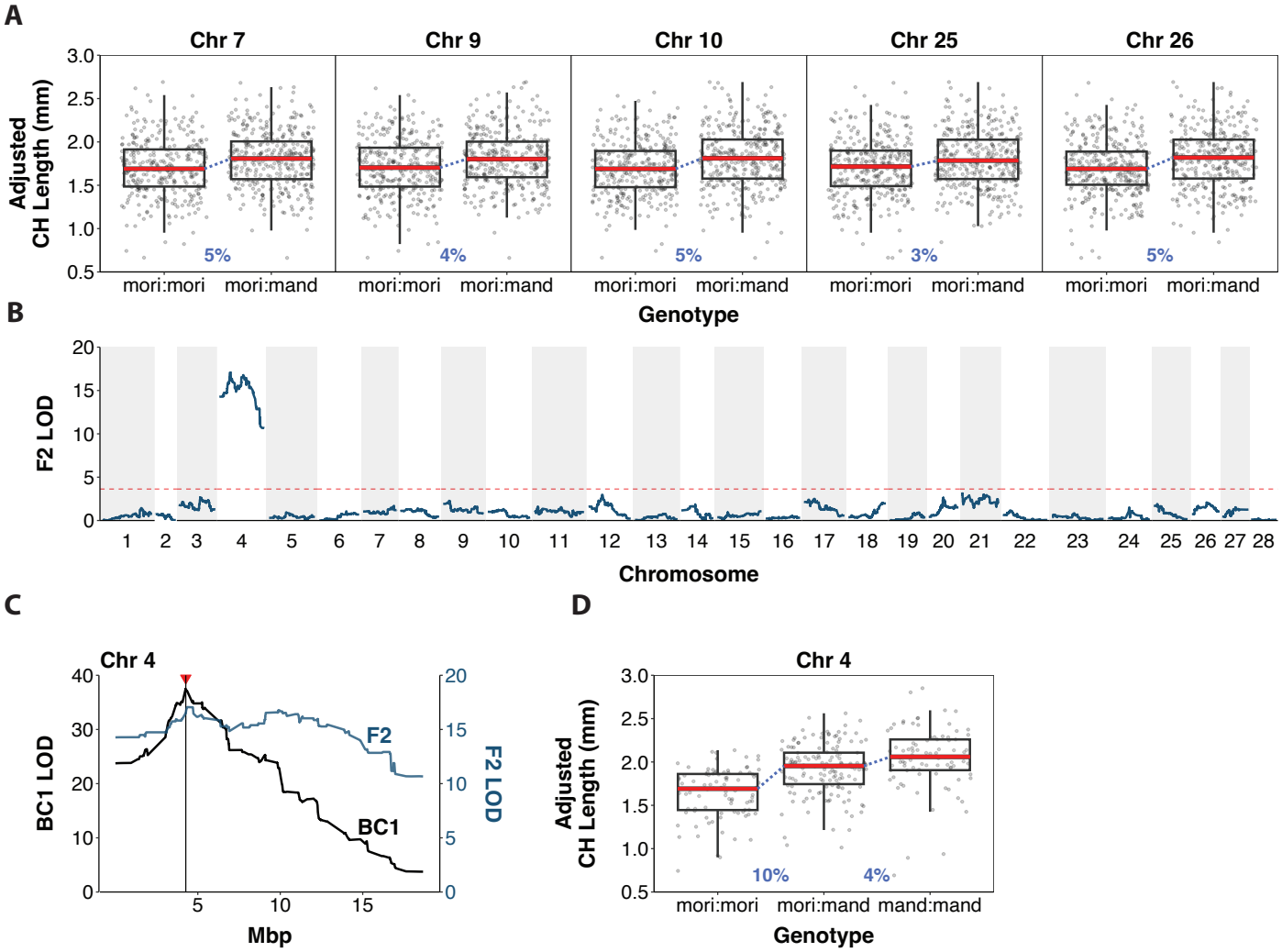
A
Chr 7
Chr 9
Chr 10
Chr 25
Chr 26
Adjusted CH Length (mm)
3.0
2.5
2.0
1.5
1.0
0.5
5%
4%
5%
3%
5%
mori:mori
mori:mand
Genotype
B
F2 LOD
20
15
10
5
0
1 2 3 4 5 6 7 8 9 10 11 12 13 14 15 16 17 18 19 20 21 22 23 24 25 26 27 28
Chromosome
C
Chr 4
BC1 LOD
F2 LOD
F2
BC1
40
30
20
10
0
5
10
15
Mbp
D
Chr 4
Adjusted CH Length (mm)
10%
4%
mori:mori
mori:mand
mand:mand
Genotype

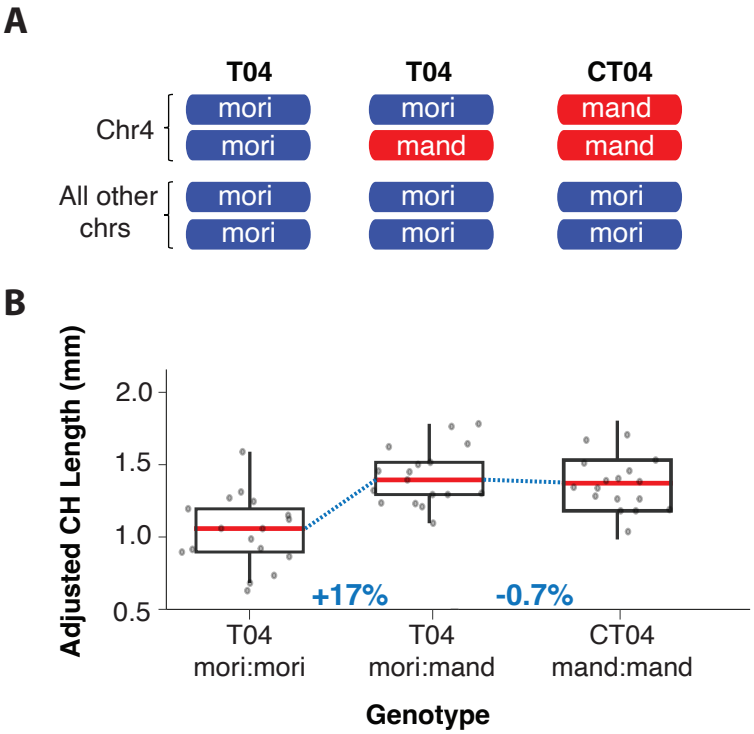
A
T04
T04
CT04
Chr4
mori
mori
mori
mand
mand
mand
All other chrs
mori
mori
mori
mori
mori
mori
B
Adjusted CH Length (mm)
2.0
1.5
1.0
0.5
+17%
-0.7%
T04 mori:mori
T04 mori:mand
CT04 mand:mand
Genotype

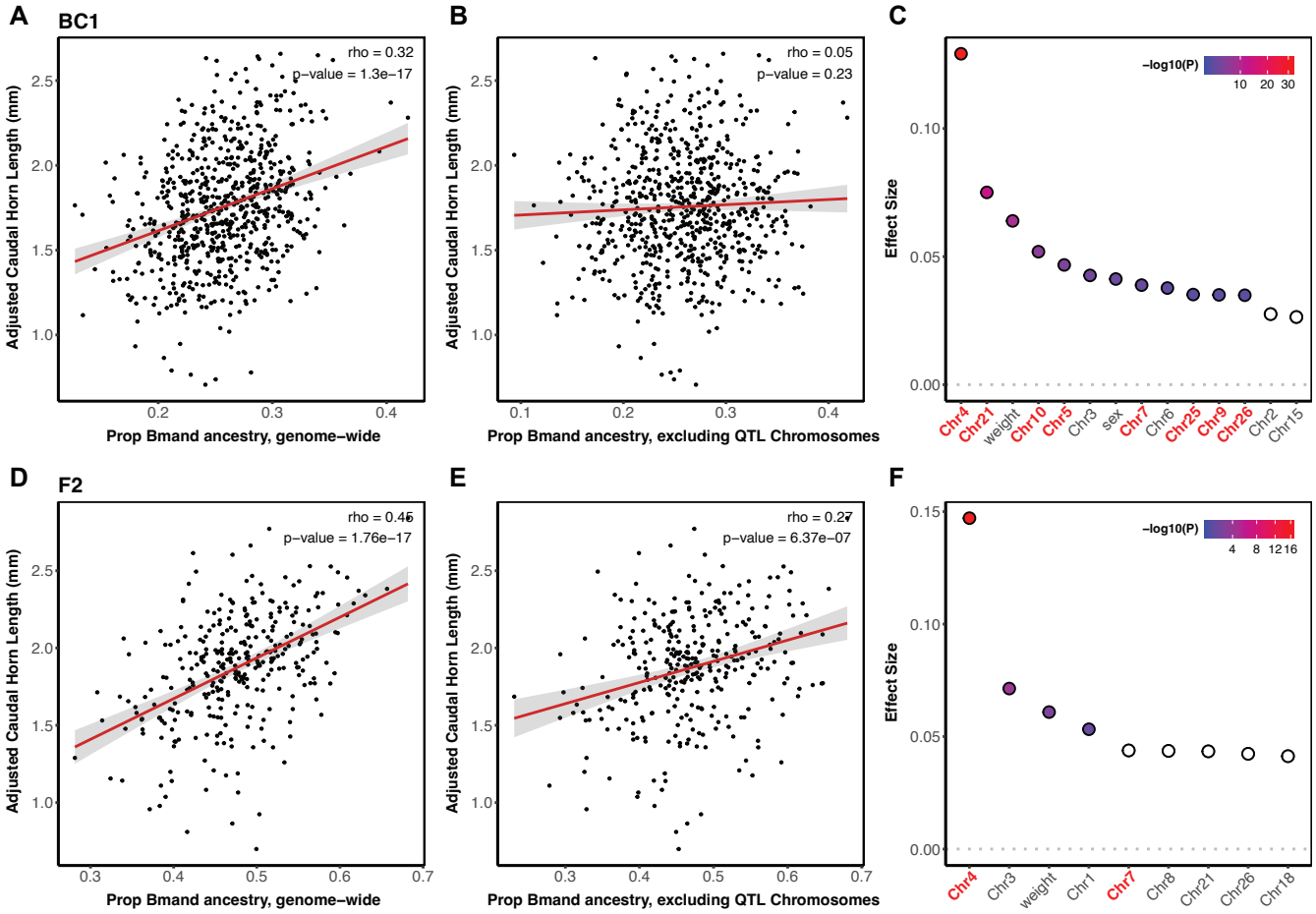
A
BC1
rho = 0.32
p−value = 1.3e−17
Adjusted Caudal Horn Length (mm)
Prop Bmand ancestry, genome−wide
B
rho = 0.05
p−value = 0.23
Adjusted Caudal Horn Length (mm)
Prop Bmand ancestry, excluding QTL Chromosomes
C
−log10(P)
10 20 30
Effect Size
Chr4
Chr21
weight
Chr10
Chr5
Chr3
sex
Chr7
Chr6
Chr25
Chr9
Chr26
Chr2
Chr15
D
F2
rho = 0.46
p−value = 1.76e−17
Adjusted Caudal Horn Length (mm)
Prop Bmand ancestry, genome−wide
E
rho = 0.27
p−value = 6.37e−07
Adjusted Caudal Horn Length (mm)
Prop Bmand ancestry, excluding QTL Chromosomes
F
−log10(P)
4 8 12 16
Effect Size
Chr4
Chr3
weight
Chr1
Chr7
Chr8
Chr21
Chr26
Chr18

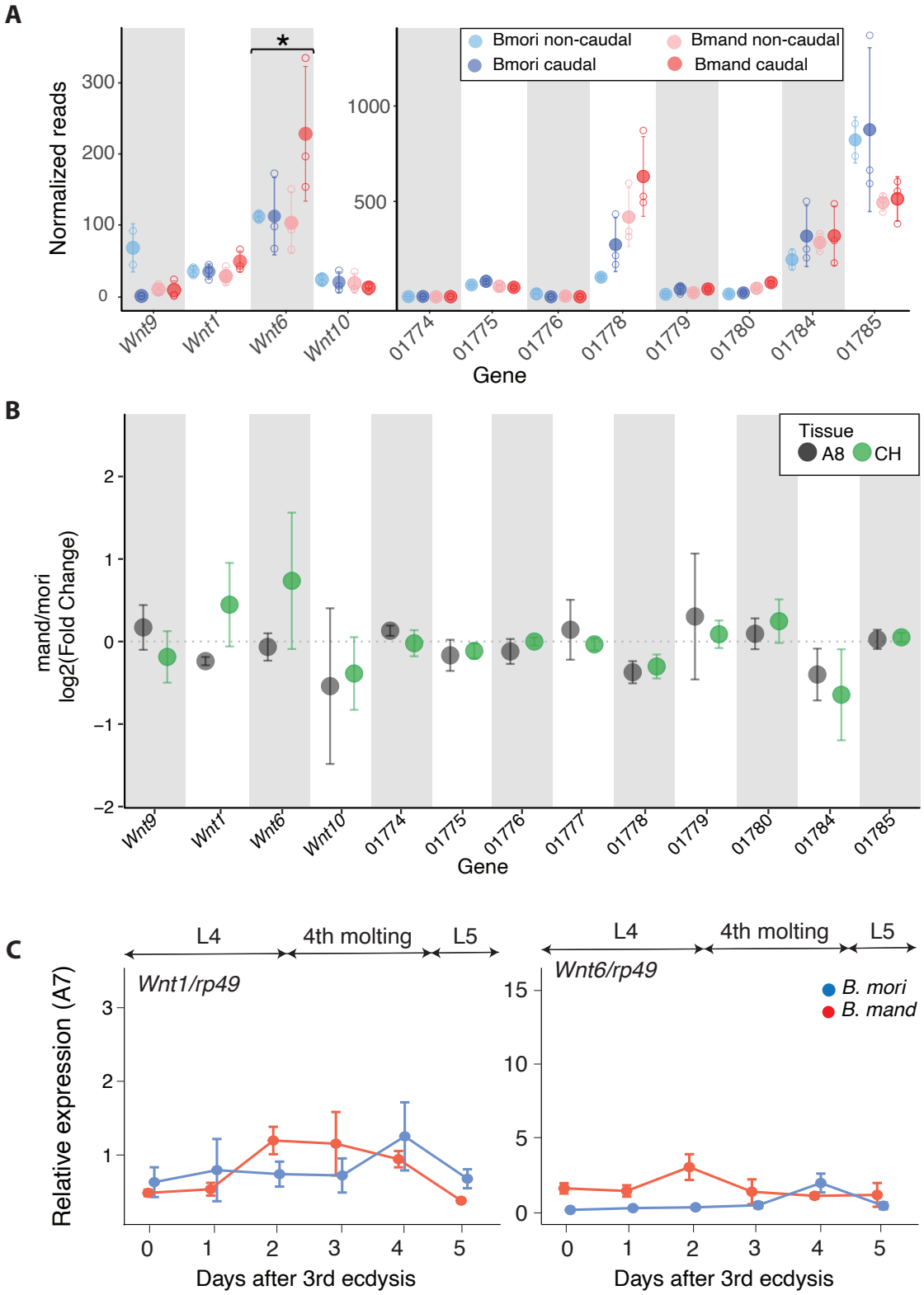
A
Normalized reads
Bmori non-caudal
Bmori caudal
Bmand non-caudal
Bmand caudal
*
Wnt9
Wnt1
Wnt6
Wnt10
01774
01775
01776
01778
01779
01780
01784
01785
Gene
B
mand/mori
log2(Fold Change)
Tissue
A8
CH
Wnt9
Wnt1
Wnt6
Wnt10
01774
01775
01776
01777
01778
01779
01780
01784
01785
Gene
C
L4
4th molting
L5
Wnt1/rp49
Wnt6/rp49
B. mori
B. mand
Relative expression (A7)
Days after 3rd ecdysis

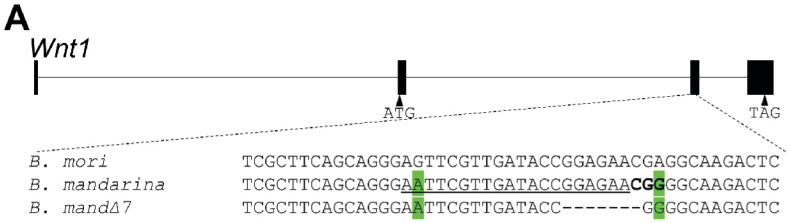
A
Wnt1
ATG
TAG
B. mori TCGCTTCAGCAGGGAGTTCGTTGATACCGGAGAACGAGGCAAGACTC
B. mandarina TCGCTTCAGCAGGGAATTCGTTGATACCGGAGAACGGGGCAAGACTC
B. mandΔ7 TCGCTTCAGCAGGGAATTCGTTGATACC-------GGGGCAAGACTC

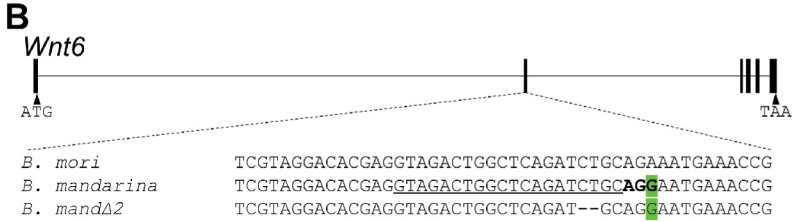
B
Wnt6
ATG
TAA
B. mori TCGTAGGACACGAGGTAGACTGGCTCAGATCTGCAGAAATGAAACCG
B. mandarina TCGTAGGACACGAGGTAGACTGGCTCAGATCTGCAGGAATGAAACCG
B. mandΔ2 TCGTAGGACACGAGGTAGACTGGCTCAGAT--GCAGGAATGAAACCG

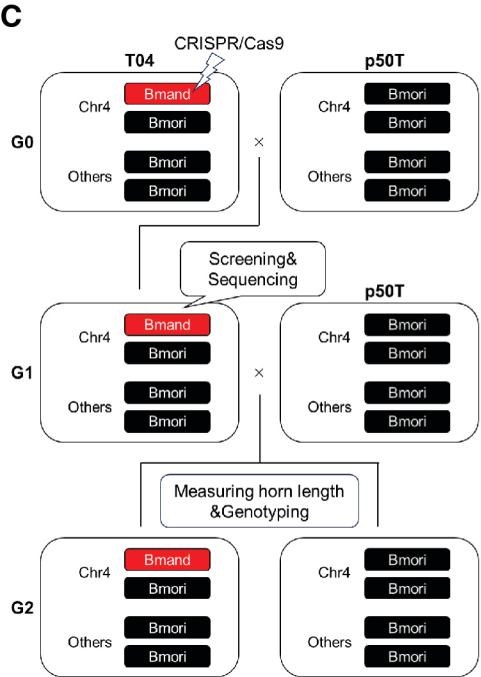
C
CRISPR/Cas9
T04
p50T
G0
Chr4
Bmand
Bmori
Others
Bmori
Bmori
×
Screening&
Sequencing
G1
Measuring horn length
&Genotyping
G2

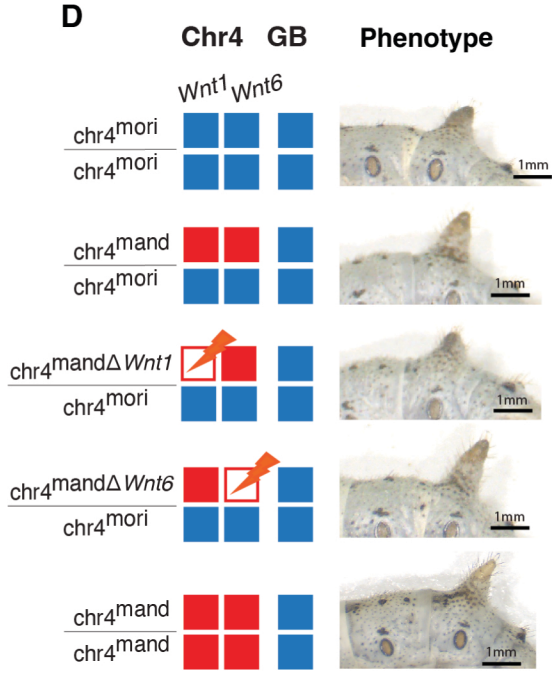
D
Chr4 GB
Phenotype
Wnt1 Wnt6
chr4mori
chr4mori
chr4mand
chr4mori
chr4mandΔWnt1
chr4mori
chr4mandΔWnt6
chr4mori
chr4mand
chr4mand
1mm